Implicit Function Based Open-loop Analysis Method for Detecting the SSR Using Identified System Parameters

Luonan Qiu, Tianhao Wen, *Member, IEEE, Member, CSEE*, Yang Liu, *Member, IEEE, Member, CSEE*, and Q. H. Wu, *Life Fellow, IEEE, Fellow, CSEE*

***Abstract*—This paper proposes an implicit function based open-loop analysis method to detect the subsynchronous resonance(SSR), including asymmetric subsynchronous modal attraction(ASSMA) and asymmetric subsynchronous modal repulsion(ASSMR), of doubly-fed induction generator based wind farms(DFIG-WFs) penetrated power systems. As some important parameters of DFIG-WF are difficult to obtain, reinforcement learning and least squares method are applied to identify those important parameters. By predicting the location of closed-loop subsynchronous oscillation(SSO) modes based on the calculation of partial differentials of characteristic equation, both ASSMA and ASSMR can be found. The proposed method in this paper can select SSO modes which move to the right half complex planes as control parameters change. Besides, the proposed open-loop analysis method is adaptive to parameter uncertainty. Simulation studies are carried out on the 4-machine 11-bus power system to verify properties of the proposed method.**

***Index Terms*—Open-loop modal analysis, reinforcement learning based parameter identification, subsynchronous resonance.**

NOMENCLATURE

R_{s}	Stator resistance of DFIG-WF.
L_{s}	Stator inductance of DFIG-WF.
R_{r}	Rotor resistance of DFIG-WF.
L_{r}	Rotor inductance of DFIG-WF.
L_{m}	Mutual inductance of DFIG-WF.
R_{c}	Resistance of the RL filter in DFIG-WF.
L_{c}	Inductance of the RL filter in DFIG-WF.
C	DC-link capacitance of DFIG-WF.
H_{g}	Generator inertia constant.
H_{t}	Turbine inertia constant.
D_{t}	Turbine damping coefficient.
D_{g}	Generator damping coefficient.
D_{tg}	Shaft mutual damping coefficient.
K_{tg}	Shaft spring constant.
$\tilde{a}$	estimate of a by using parameter identification method.

Manuscript received July 27, 2021; revised November 4, 2021; accepted December 5, 2021. Date of online publication November 17, 2023; date of current version December 26, 2023. This work was supported in part by the State Key Program of National Natural Science Foundation of China under Grant No. U1866210, and the National Natural Science Foundation of China under Grant No. 51807067.

L. N. Qiu, T. H. Wen, Y. Liu (corresponding author, email: epyangliu@scut.edu.cn), and Q. H. Wu are with the School of Electric Power Engineering, South China University of Technology, Guangzhou 510640, China.

DOI: 10.17775/CSEEJPES.2021.05480

I. INTRODUCTION

IN recent years, large-scale wind power plants have been increasingly integrated into power systems. However, open-loop modal proximity [1] between the subsynchronous oscillation (SSO) modes of wind farm (WF) subsystem and the SSO modes of *the rest of power system* (ROPS) subsystem [1] may cause subsynchronous resonance (SSR) in the entire power system. SSR is worthy of being detected as it greatly affect small-signal stability of power system. So far, methods for investigation of SSR between WF subsystem and ROPS subsystem include modal analysis [2], damping torque analysis(DTA) [3]–[5], small-signal impedance method [6], [7], open-loop analysis method [1] and residue based method [8].

Modal analysis is a widely applied method of studying SSR of power system [9]. Modal analysis has been applied to the entire WF penetrated power system, and can indicate roles of the WF subsystem and the ROPS subsystem in affecting the system's small-signal stability by calculating participation factors of states. However, it is difficult for the method to reveal the mechanism which determines the influence of selected WFs on small-signal stability of the entire power system. Furthermore, it is time-consuming for the method to perform stability analysis due to the high dimension of the state matrix of entire power system.

In addition, DTA is another method to study impact of SSR on power system small-signal stability. In [10], DTA was used to exam open-loop modal proximity between electromechanical oscillation modes (EOMs) of an AC power system and oscillation modes of the integrated multi-terminal DC (MTDC) network. In [5], DTA is adopted to study SSR damping characteristics with SVC. An investigation on the mechanism about how and why SVC can effectively provide damping to SSR is presented. Although the physical meaning of DTA method is clear, it cannot find the exact location of SSO modes on the complex plane.

Recently, other methods of studying SSR have been put forward, such as small-signal impedance method and the open-loop analysis method proposed in [1]. In [6], small-signal impedance method has been used to analyze multiple high-frequency resonances (MHFR) between the DFIG system and series Π-sections weak network. An active damping strategy which introduces a virtual impedance, including a phase leading compensation unit and a virtual positive resistance, was proposed there to mitigate the MHFR. Besides, [7] utilized small-signal impedance method to study high-frequency resonance between DFIG-based offshore wind farm and long transmission cable.

The open-loop analysis method identifies any pair of open-loop SSO modes close to each other from two open-loop subsystems. An index, indicator of the strength of symmetric modal repulsion [8] of the identified open-loop modes, is calculated without using the information of closed-loop eigenvalues. However, the method is only suitable for analyzing symmetric modal resonance [8]. In particular, location of closed-loop SSO modes and small-signal stability margin it gives are correct only when the identified pair of open-loop modes are equal [8]. Besides, the mechanism of SSR, especially asymmetric subsynchronous modal attraction(ASSMA) and asymmetric subsynchronous modal repulsion(ASSMR), has not been intensively analyzed in [1], [11], [12]. Last, but not least, the open-loop analysis method proposed in [1] is not adaptive to parameter uncertainty.

The above-mentioned problems have been partially solved by paper [8]. In [8], the mechanism of modal resonance, especially modal repulsion and modal attraction, has been intensively analyzed. A residue based analysis method has been proposed there to detect asymmetric modal resonance [8] via estimating locations of selected closed-loop modes. However, estimation error of the locations of closed-loop mode still exists. The method studied in [8] is still not adaptive to parameter uncertainty.

In order to improve accuracy of small-signal analysis when some important system parameters are difficult to obtain directly, parameter identification methods can be utilized [8]. Existing parameter identification methods include least squares method [13], [14], reinforcement learning method [15], Kalman filter based method, etc. Among those methods, least squares method is easier to implement. However, it cannot be directly used to identify parameters of DFIG, according to the mathematic model of the generator. Reinforcement learning method can be used to identify parameters of equipment with complex structure. But it suffers from high computational complexity [8].

Contributions of this paper consist of three aspects. First of all, a model for analyzing SSR of DFIG-WFs integrated power system is derived. The model consists of DFIG subsystem and ROPS subsystem [8]. In addition, reinforcement learning and least squares method are applied to identify parameters of DFIG subsystem, which are difficult to obtain. Furthermore, an implicit function based open-loop analysis method is proposed to detect ASSMA and ASSMR by estimating locations of selected closed-loop SSO modes of the entire power system. Compared with the residue based open-loop modal analysis method mentioned in [8], the proposed method is adaptive to variation of system parameters. A DFIG-WFs integrated 4-machine 11-bus power system is used to demonstrate performances of the proposed method.

II. ASSMA and ASSMR Caused by DFIG

A. A Closed-Loop Model of DFIG-WFs Integrated Power System for Analyzing SSR

Figure 1 shows a multi-machine power system with p DFIG-WFs, where $I_{\mathrm{x}k} + \mathrm{j}I_{\mathrm{y}k}$ $(k = 1, 2, \cdots, p)$ denotes the output current of the kth DFIG-WF and $V_{\mathrm{x}k} + \mathrm{j}V_{\mathrm{y}k}$ $(k = 1, 2, \cdots, p)$ denotes terminal voltage of the kth DFIG-WF, expressed in the common x-y coordinate. The system can be divided into DFIG subsystem and ROPS subsystem [8]. As for DFIG subsystem, its open-loop linearized state-space model is:

$$\begin{cases} \frac{\mathrm{d}}{\mathrm{d}t}\Delta \boldsymbol{X}_{\mathrm{d}} = \boldsymbol{A}_{\mathrm{d}}\Delta \boldsymbol{X}_{\mathrm{d}} + \boldsymbol{B}_{\mathrm{d}}\Delta \boldsymbol{V}_{\mathrm{xy}} \\ \Delta I_{\mathrm{xy}} = \boldsymbol{C}_{\mathrm{d}}\Delta \boldsymbol{X}_{\mathrm{d}} \end{cases} \tag{1}$$

where

$$\boldsymbol{A}_{\mathrm{d}} = \begin{pmatrix} \boldsymbol{A}_{\mathrm{d1}} & 0 & \cdots & \cdots & \cdots & 0 \\ 0 & \boldsymbol{A}_{\mathrm{d2}} & 0 & & & \vdots \\ \vdots & 0 & \ddots & & & \vdots \\ \vdots & & & \boldsymbol{A}_{\mathrm{d}k} & & \vdots \\ \vdots & & & & \ddots & 0 \\ 0 & \cdots & \cdots & \cdots & 0 & \boldsymbol{A}_{\mathrm{d}p} \end{pmatrix}$$

$\boldsymbol{A}_{\mathrm{d}k}$ is state matrix of the kth DFIG-WF, $\boldsymbol{X}_{\mathrm{d}}$ is vector of all state variables of p DFIG-WFs, and prefix Δ indicates small variation of variable(s). Note each wind farm is modelled as an aggregated DFIG-based wind turbine (DFIG-WT) [8]. According to (1), the transfer function matrix of DFIG subsystem can be written as:

$$\Delta I_{\mathrm{xy}} = D(s)\Delta V_{\mathrm{xy}} \tag{2}$$

where

$$\begin{aligned} \Delta I_{\mathrm{xy}} &= [\Delta I_{\mathrm{x1}} \quad \Delta I_{\mathrm{y1}} \quad \cdots \quad \Delta I_{\mathrm{x}p} \quad \Delta I_{\mathrm{y}p}]^{\mathrm{T}} \\ \Delta V_{\mathrm{xy}} &= [\Delta V_{\mathrm{x1}} \quad \Delta V_{\mathrm{y1}} \quad \cdots \quad \Delta V_{\mathrm{x}p} \quad \Delta V_{\mathrm{y}p}]^{\mathrm{T}} \\ D(s) &= C_{\mathrm{d}}(sI - A_{\mathrm{d}})^{-1}B_{\mathrm{d}} \end{aligned} \tag{3}$$

and I is the identity matrix of proper dimension. As for ROPS subsystem, its open-loop linearized state equation can be written as [8]:

$$\begin{cases} \frac{\mathrm{d}}{\mathrm{d}t}\Delta X_{\mathrm{r}} = A_{\mathrm{r}}\Delta X_{\mathrm{r}} + B_{\mathrm{r}}\Delta I_{\mathrm{xy}} \\ \Delta V_{\mathrm{xy}} = C_{\mathrm{r}}\Delta X_{\mathrm{r}} + D_{\mathrm{r}}\Delta I_{\mathrm{xy}} \end{cases} \tag{4}$$

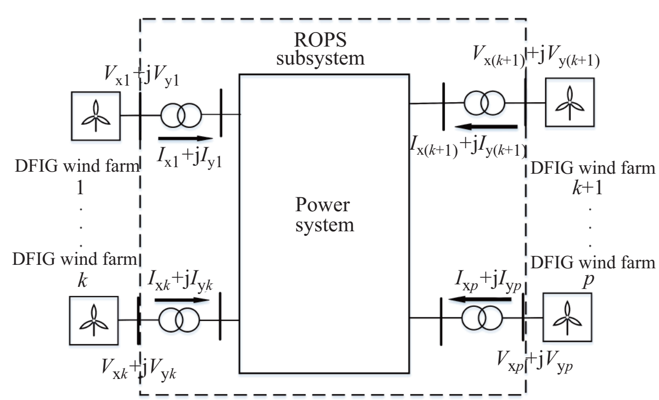

Fig. 1. A multi-machine power system with p DFIG wind farms.

where X_{r} is the vector of all the state variables of ROPS subsystem, and A_{r} is the state matrix of ROPS subsystem. The transfer function matrix of ROPS subsystem is:

$$\Delta V_{\mathrm{xy}} = R(s)\Delta I_{\mathrm{xy}} \tag{5}$$

where

$$R(s) = C_{\mathrm{r}}(sI - A_{\mathrm{r}})^{-1}B_{\mathrm{r}} + D_{\mathrm{r}} \tag{6}$$

In order to calculate the residue of open-loop modes of DFIG subsystem, the multi-machine power system should be regarded as the feedback connection of DFIG subsystem and ROPS subsystem, as shown in Fig. 2 [8]. However, in order to calculate the residue of open-loop modes of ROPS subsystem, virtual transfer functions $D'(s)$ and $R'(s)$ should be introduced, since $D_{\mathrm{r}} \neq \boldsymbol{O}$, according to *the hybrid formulation for the sensitivity* [16]. At the same time, the multi-machine power system needs to be treated as the feedback connection of a modified ROPS subsystem and a modified DFIG subsystem, as demonstrated in Fig. 3 [8]. $D'(s)$, $R'(s)$ in Fig. 3 are derived as:

$$\begin{aligned} D'(s) &= C_{\mathrm{d}}(sI - A_{\mathrm{d}})^{-1}B_{\mathrm{d}}[I - D_{\mathrm{r}}D(s)]^{-1} \\ R'(s) &= R(s) - D_{\mathrm{r}} \\ \Delta V'_{\mathrm{xy}} &= [I - D_{\mathrm{r}}D(s)]\Delta V_{\mathrm{xy}} \end{aligned} \tag{7}$$

Besides, the linearized closed-loop model of the entire power system can be presented as:

$$\frac{\mathrm{d}}{\mathrm{d}t}\Delta X = A\Delta X \tag{8}$$

where

$$\begin{aligned} \Delta X &= [\Delta X_{\mathrm{r}}^{\mathrm{T}} \quad \Delta X_{\mathrm{d}}^{\mathrm{T}}]^{\mathrm{T}} \\ A &= \begin{bmatrix} A_{\mathrm{d}} + B_{\mathrm{d}}D_{\mathrm{r}}C_{\mathrm{d}} & B_{\mathrm{d}}C_{\mathrm{r}} \\ B_{\mathrm{r}}C_{\mathrm{d}} & A_{\mathrm{r}} \end{bmatrix} \end{aligned} \tag{9}$$

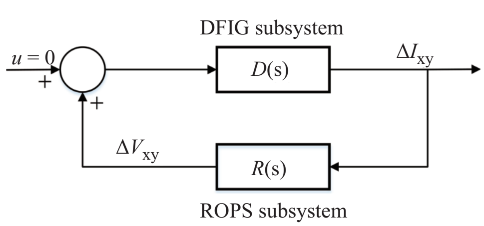

Fig. 2. Closed-loop model for calculation of residue of open-loop modes of DFIG subsystem.

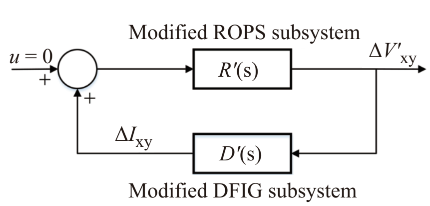

Fig. 3. Closed-loop model for calculation of residue of open-loop modes of ROPS subsystem.

B. Identification of Parameters of DFIG Subsystem

As several parameters of DFIG-WF are difficult to obtain directly, reinforcement learning [17] and least-square method [18] are applied to identify them. While K_{tg} is identified via reinforcement learning, other parameters listed below are estimated via least-square method.

$$[R_{\mathrm{s}}, L_{\mathrm{s}}, R_{\mathrm{r}}, L_{\mathrm{r}}, L_{\mathrm{m}}, R_{\mathrm{c}}, L_{\mathrm{c}}, C, H_{\mathrm{g}}, H_{\mathrm{t}}, D_{\mathrm{t}}, D_{\mathrm{g}}, D_{\mathrm{tg}}]$$

1) Identification of K_{tg} Via Reinforcement Learning

The reinforcement learning based parameter identification [17], [19] consists of two key steps. The first key step is to sample the measurable state variable ω_{t} within a certain time interval. The second key step is to make comparisons between the sampled values and simulated values of ω_{t}. Simulated values of ω_{t} are obtained from simulating the following differential equation via improved euler method.

$$\begin{aligned} T_{\mathrm{m}} &= \frac{P_{\mathrm{m}}}{\omega_{\mathrm{t}}} \\ \frac{\mathrm{d}}{\mathrm{d}t}\omega_{\mathrm{t}} &= \frac{(-D_{\mathrm{g}} - D_{\mathrm{tg}})\omega_{\mathrm{t}} + D_{\mathrm{tg}}\omega_{\mathrm{r}} - T_{\mathrm{g}} + T_{\mathrm{m}}}{2H_{\mathrm{t}}} \\ \frac{\mathrm{d}}{\mathrm{d}t}T_{\mathrm{g}} &= 120\pi K_{\mathrm{tg}}(\omega_{\mathrm{t}} - \omega_{\mathrm{r}}) \end{aligned} \tag{10}$$

Parameters in (10) are replaced by their identified values. To find an optimal result of identification, an objective function is constructed as:

$$\begin{aligned} F &= \frac{10\sqrt{\sum_{i=1}^{\mathrm{s}}(\tilde{\omega}_{\mathrm{t}}^{i} - \omega_{\mathrm{t}}^{i})^2}}{\sum_{i=1}^{\mathrm{s}}(\omega_{\mathrm{t}}^{i})^2} + F_{\mathrm{pi}} \\ F_{\mathrm{pi}} &= \max(-H_{\mathrm{t}}, 0) + \max(-K_{\mathrm{tg}} + 300, 0) + \\ &\quad \max(-D_{\mathrm{t}}, 0) + \max(-D_{\mathrm{tg}}, 0) + \max(-T_{\mathrm{g0}}, 0) \end{aligned} \tag{11}$$

where s is total number of sampling points, T_{g0} is an estimate of the value of T_{g} at the beginning of the sample interval, a^{i} is value of variable a at the ith sampling time, $\tilde{a}$ is simulated value of variable a. and F_{pi} is penalty item aiming at avoiding parameters falling into unreasonable range. By using genetic algorithm to obtain minimum of the objective function, the best estimate of K_{tg} can be obtained.

2) Identification of Remaining Parameters of DFIG-WF Using Least Squares Method

Once the identified value of K_{tg} and the best estimate of T_{g} are obtained, other parameters of DFIG-WF can be identified via least square method [18]–[20]. The least square method is based on linear identification equations demonstrated in the appendix, which are originated from the backward difference of the state equation of DFIG-WF.

In order for identification to work properly, $i_{x\mathrm{s}}$, $i_{y\mathrm{s}}$, $i_{x\mathrm{r}}$, $i_{y\mathrm{r}}$, $i_{x\mathrm{c}}$, $i_{y\mathrm{c}}$, $V_{x\mathrm{s}}$, $V_{y\mathrm{s}}$, $V_{x\mathrm{r}}$, $V_{y\mathrm{r}}$, $V_{x\mathrm{c}}$, $V_{y\mathrm{c}}$, ω_{t}, T_{g}, ω_{r} and U_{dc} should be measured. Because it is difficult for T_{g} to be measured directly, T_{g} is replaced by $\tilde{T}_{\mathrm{g}}$. Moreover, the square deviation of the linear identification equations can be written as:

$$\delta = \sum_{i=1}^{\mathrm{s}}\sum_{j=1}^{9}(z_{i,j,1}k_1 + z_{i,j,2}k_2 + \cdots + z_{i,j,21}k_{21} - v_{i,j})^2 \tag{12}$$

where $z_{i,j,m}$ $(m = 1, \cdots, 21)$ are the coefficients of k_{m} in jth equation of (12) related to value of variables at the ith sampling time, and $v_{i,j}$ represents the left-hand side of the ith equation of (A1), taking values at the ith sampling time. After finding the least square solution of (A1) for $k_1, k_2, \cdots, k_{21}$, identified values of parameters $\tilde{R}_{\rm s}, \tilde{L}_{\rm s}, \tilde{R}_{\rm r}, \tilde{L}_{\rm r}, \tilde{L}_{\rm m}, \tilde{R}_{\rm c}, \tilde{L}_{\rm c}, \tilde{C}$, $\tilde{H}_{\rm g}, \tilde{H}_{\rm t}, \tilde{D}_{\rm t}, \tilde{D}_{\rm g}$ and $\tilde{D}_{\rm tg}$ can be obtained from (A2).

C. Formation of ASSMA and ASSMR

Normally, dynamic interactions between DFIG subsystem and ROPS subsystem are weak. As a result, DFIG subsystem and ROPS subsystem can be recognized as almost decoupled. This recognition has been explained in [11]. Therefore, within the range of the frequency of SSO, $\Delta V_{\rm xy} \approx \mathbf{0}$ and $\Delta V'_{\rm xy} \approx \mathbf{0}$. Based on this supposition, a small positive number ξ, $0 < \xi \ll 1$, can be introduced in the transfer function matrix of the ROPS subsystem and it can be expressed as $R(s) = \xi X(s)$ [8], where

$$\begin{aligned} R(s) &= \xi X(s) = \frac{\xi x(s)}{s-\lambda_{{\rm g}i}} \\ D(s) &= \frac{d(s)}{s-\lambda_{{\rm w}h,i}} \\ \xi x(s) &= R_{{\rm g}i} + (s-\lambda_{{\rm g}i})\left(\sum_{j=1,j\neq i}^{n_{\rm g}} \frac{R_{{\rm g}j}}{s-\lambda_{{\rm g}j}} + D_{\rm r}\right) \\ d(s) &= R_{{\rm w}h,i} + (s-\lambda_{{\rm w}h,i})\left(\sum_{j=1,j\neq i}^{n_{{\rm w}h}} \frac{R_{{\rm w}h,j}}{s-\lambda_{{\rm w}h,j}}\right) + \\ &\quad (s-\lambda_{{\rm w}h,i})\left(\sum_{l=1,l\neq h}^{\rm p}\sum_{j=1}^{n_{{\rm w}l}} \frac{R_{{\rm w}l,j}}{s-\lambda_{{\rm w}l,j}}\right) \end{aligned} \tag{13}$$

$\lambda_{{\rm g}i}$ is ith eigenvalue of $A_{\rm r}$; $\lambda_{{\rm w}h,i}$ $(h = 1, \cdots, p, i = 1, \cdots, n_{{\rm w}h})$ is ith eigenvalue of $A_{{\rm d}h}$; $n_{\rm g}$ is dimension of $A_{\rm r}$; $n_{{\rm w}h}$ is dimension of $A_{{\rm d}h}$, $R_{{\rm g}i} = C_{\rm r} v_{{\rm g}i} w_{{\rm g}i}^{\rm T} B_{\rm r}$, $R_{{\rm w}h,i} = C_{\rm d} v_{{\rm w}h,i} w_{{\rm w}h,i}^{\rm T} B_{\rm d}$; $v_{{\rm g}i}$ is right eigenvector corresponding to $\lambda_{{\rm g}i}$; $w_{{\rm g}i}$ is left eigenvector corresponding to $\lambda_{{\rm g}i}$; $v_{{\rm w}h,i}$ is right eigenvector of $A_{\rm d}$ corresponding to $\lambda_{{\rm w}h,i}$; and $w_{{\rm w}h,i}$ is left eigenvector of $A_{\rm d}$ corresponding to $\lambda_{{\rm w}h,i}$.

According to [21], all eigenvalues of A are continuously differentiable with respect to ξ. When $\xi = 0$, eigenvalues of A are composed of eigenvalues of $A_{\rm r}$ and $A_{\rm d}$. To be more specific, for $\lambda_{{\rm g}i}$, also an eigenvalue of A when $\xi = 0$, it moves to $\hat{\lambda}_{{\rm g}i}$ as ξ becomes positive. Moreover according to [12], $\Delta\lambda_{{\rm g}i} = \hat{\lambda}_{{\rm g}i} - \lambda_{{\rm g}i}$ can be approximately expressed as [8]:

$$\Delta\lambda_{{\rm g}i} \approx \xi \frac{{\rm tr}[d(\lambda_{{\rm g}i}) x(\lambda_{{\rm g}i})]}{\lambda_{{\rm g}i} - \lambda_{{\rm w}h,i}} \tag{14}$$

where ${\rm tr}(A)$ denotes the trace of matrix A. Similarly, for $\Delta\lambda_{{\rm w}h,i} = \hat{\lambda}_{{\rm w}h,i} - \lambda_{{\rm w}h,i}$, it can be derived that

$$\Delta\lambda_{{\rm w}h,i} \approx \xi \frac{{\rm tr}[d(\lambda_{{\rm w}h,i}) x(\lambda_{{\rm w}h,i})]}{\lambda_{{\rm w}h,i} - \lambda_{{\rm g}i}} \tag{15}$$

When $\lambda_{{\rm g}i}$ is not close to $\lambda_{{\rm w}h,i}$, equations (14) and (15) show under the condition of $0 < \xi \ll 1$ $\Delta\lambda_{{\rm g}i}$ and $\Delta\lambda_{{\rm w}h,i}$ are small. However, as system parameters or operating condition vary, $\lambda_{{\rm g}i}$ may become close to $\lambda_{{\rm w}h,i}$, causing $\Delta\lambda_{{\rm g}i}$ and $\Delta\lambda_{{\rm w}h,i}$ to become significant. Such phenomenon is called SSR [8], if the imaginary part of $\lambda_{{\rm g}i}$ and $\lambda_{{\rm w}h,i}$ are within range of the frequency of SSO when $|\lambda_{{\rm g}i} - \lambda_{{\rm w}h,i}|$ is small. Note the difference between SSR and low frequency modal resonance (LFMR) studied in [8] is that LFMR occurs when the imaginary part of $\lambda_{{\rm g}i}$ and $\lambda_{{\rm w}h,i}$ are within range of the frequency of low frequency oscillation (LFO). As for SSO, $\lambda_{{\rm g}i}$ and $\lambda_{{\rm w}h,i}$ are defined as the pair of open-loop SSO modes participating in the SSR. $\hat{\lambda}_{{\rm g}i}$ and $\hat{\lambda}_{{\rm w}h,i}$ are considered to be the corresponding pair of closed-loop SSO modes [8]. As for a specified parameter set in parameter space, if the following requirements on the pair of open-loop SSO modes can fulfill as system parameters vary within the set [8],

$$\begin{aligned} \lambda_{{\rm g}i} &= \lambda_{{\rm w}h,i} \\ \Delta\lambda_{{\rm g}i} &= \Delta\lambda_{{\rm w}h,i} \end{aligned} \tag{16}$$

then SSR occurred in the system is considered to be symmetric. Otherwise, SSR occurred in the system is regarded as asymmetric [8]. As for asymmetric SSR, within the parameter set, there is a group of parameters, under which $|\lambda_{{\rm g}i} - \lambda_{{\rm w}h,i}|$ reaches the minimum [8]. That group of parameters correspond to a parameter vector in the parameter space, and endpoint of the vector is defined as near open-loop modal resonance(NOLMR) point. Once the endpoint of the parameter vector of the system reaches the NOLMR point [8], if

$${\rm Re}(\lambda_{{\rm w}h,i}) < {\rm Re}(\lambda_{{\rm g}i}),\ {\rm Re}(\Delta\lambda_{{\rm g}i}) < 0$$

or

$${\rm Re}(\lambda_{{\rm w}h,i}) > {\rm Re}(\lambda_{{\rm g}i}),\ {\rm Re}(\Delta\lambda_{{\rm g}i}) > 0$$

then ASSMA happens in the system. On the other hand, if

$${\rm Re}(\lambda_{{\rm w}h,i}) < {\rm Re}(\lambda_{{\rm g}i}),\ {\rm Re}(\Delta\lambda_{{\rm g}i}) > 0$$

or

$${\rm Re}(\lambda_{{\rm w}h,i}) > {\rm Re}(\lambda_{{\rm g}i}),\ {\rm Re}(\Delta\lambda_{{\rm g}i}) < 0$$

then ASSMR occurs in the system. In comparison to symmetric SSR, it is much easier for asymmetric SSR to occur in power system.

D. Estimation of ASSMA and ASSMR

For detecting ASSMA and ASSMR, an implicit function based open-loop analysis method is proposed to estimate locations of closed-loop SSO modes. The proposed method relies on information of partial derivatives of real and imaginary parts of the characteristic equation as well as residue of open-loop SSO modes. Detailed derivations of the proposed method are presented as follows.

Assume $\lambda_{{\rm g}i}$ and $\lambda_{{\rm w}h,i}$ are the identified pair of open-loop modes participating in the SSR. Then, for $R(s)$ and $D(s)$ in Fig. 2, they can be expressed as:

$$\begin{aligned} R(s) &= \frac{R_{{\rm g}i}}{s-\lambda_{{\rm g}i}} + \sum_{j=1,j\neq i}^{n_{\rm g}} \frac{R_{{\rm g}j}}{s-\lambda_{{\rm g}j}} + D_{\rm r} \\ D(s) &= \frac{R_{{\rm w}h,i}}{s-\lambda_{{\rm w}h,i}} + \sum_{j=1,j\neq i}^{n_{{\rm w}h}} \frac{R_{{\rm w}h,j}}{s-\lambda_{{\rm w}h,j}} \\ &\quad + \sum_{l=1,l\neq h}^{\rm p}\sum_{j=1}^{n_{{\rm w}l}} \frac{R_{{\rm w}l,j}}{s-\lambda_{{\rm w}l,j}} \end{aligned} \tag{17}$$

For $R'(s)$ and $D'(s)$ in Fig. 3, they can be written as:

$$\begin{aligned}
R'(s) &= \left(\frac{R_{\mathrm{g}i}}{s-\lambda_{\mathrm{g}i}} + \sum_{j=1, j\neq i}^{n_{\mathrm{g}}} \frac{R_{\mathrm{g}j}}{s-\lambda_{\mathrm{g}j}}\right) \\
D'(s) &= \Bigg(\frac{R_{\mathrm{wh},i}}{s-\lambda_{\mathrm{wh},i}} + \sum_{j=1, j\neq i}^{n_{\mathrm{wh}}} \frac{R_{\mathrm{wh},j}}{s-\lambda_{\mathrm{wh},j}} + \\
&\quad \sum_{l=1, l\neq h}^{\mathrm{p}} \sum_{j=1}^{n_{\mathrm{w}l}} \frac{R_{\mathrm{w}l,j}}{s-\lambda_{\mathrm{w}l,j}}\Bigg)[I - D_{\mathrm{r}} D(s)]^{-1}
\end{aligned} \tag{18}$$

As for estimation of $\hat{\lambda}_{\mathrm{g}i}$, in the first place, denote:

$$\begin{aligned}
\Delta\lambda_{\mathrm{g}i} &= s - \lambda_{\mathrm{g}i} = \alpha + \mathrm{j}\beta \quad s_{\mathrm{g}i} = \nu + \mathrm{j}\kappa \\
\Gamma(\Delta\lambda_{\mathrm{g}i}) &= \left(R_{\mathrm{g}i} + \sum_{j=1, j\neq i}^{n_{\mathrm{g}}} \frac{R_{\mathrm{g}j}\cdot\Delta\lambda_{\mathrm{g}i}}{\Delta\lambda_{\mathrm{g}i} + \lambda_{\mathrm{g}i} - \lambda_{\mathrm{g}j}}\right) \\
&\quad \cdot \left(\sum_{l=1}^{\mathrm{p}} \sum_{j=1}^{n_{\mathrm{w}l}} \frac{R_{\mathrm{w}l,j}}{\Delta\lambda_{\mathrm{g}i} + \lambda_{\mathrm{g}i} - \lambda_{\mathrm{w}l,j}}\right) \\
&\quad \cdot [I - D_{\mathrm{r}} D(\Delta\lambda_{\mathrm{g}i} + \lambda_{\mathrm{g}i})]^{-1} \\
\tilde{\hat{\lambda}}_{\mathrm{g}i,\mathrm{r}} &= \lambda_{\mathrm{g}i} + w_{\mathrm{g}i}^{\mathrm{T}} B_{\mathrm{r}} D'(\lambda_{\mathrm{g}i}) C_{\mathrm{r}} v_{\mathrm{g}i} \\
\tilde{\hat{\lambda}}_{\mathrm{w}hi,\mathrm{r}} &= \lambda_{\mathrm{w}h,i} + w_{\mathrm{w}h,i}^{\mathrm{T}} B_{\mathrm{d}} R(\lambda_{\mathrm{w}h,i}) C_{\mathrm{d}} v_{\mathrm{w}h,i}
\end{aligned} \tag{19}$$

where $w_{\mathrm{g}i}^{\mathrm{T}} B_{\mathrm{r}} D'(\lambda_{\mathrm{g}i}) C_{\mathrm{r}} v_{\mathrm{g}i}$ is the residue of $\lambda_{\mathrm{g}i}$ and $w_{\mathrm{w}h,i}^{\mathrm{T}} B_{\mathrm{d}} R(\lambda_{\mathrm{w}h,i}) C_{\mathrm{d}} v_{\mathrm{w}h,i}$ is the residue of $\lambda_{\mathrm{w}h,i}$. Obviously, equation $\mathrm{Det}[(s_{\mathrm{g}i} - \lambda_{\mathrm{g}i})I - \Gamma(\Delta\lambda_{\mathrm{g}i})] = 0$ is equivalent to

$$\prod_{k=1}^{2p} (s_{\mathrm{g}i} - \lambda_{\mathrm{g}i} - \mathrm{eig}_k(\Gamma(\Delta\lambda_{\mathrm{g}i}))) = 0 \tag{20}$$

where $\mathrm{eig}_k(\Gamma)$ is the kth eigenvalue of Γ. Via the expansion of the left-hand side of (20), it can be obtained that

$$\begin{aligned}
&(s_{\mathrm{g}i} - \lambda_{\mathrm{g}i})^{2p} - (s_{\mathrm{g}i} - \lambda_{\mathrm{g}i})^{2p-1}\mathrm{tr}(\Gamma(0)) - \\
&\quad (s_{\mathrm{g}i} - \lambda_{\mathrm{g}i})^{2p-1}(\mathrm{eig}_1(\Gamma(\Delta\lambda_{\mathrm{g}i})) - \\
&\quad \mathrm{tr}(\Gamma(0))) + (s_{\mathrm{g}i} - \lambda_{\mathrm{g}i})^{2p-1}(-\mathrm{eig}_2(\Gamma(\Delta\lambda_{\mathrm{g}i}))) + \cdots + \\
&\quad (s_{\mathrm{g}i} - \lambda_{\mathrm{g}i})^{2p-1}(-\mathrm{eig}_{2p}(\Gamma(\Delta\lambda_{\mathrm{g}i}))) + (s_{\mathrm{g}i} - \lambda_{\mathrm{g}i})^{2p-2} \times \\
&\quad \sum_{\substack{\mu_k\in\{0,1\} \\ k=1,2,\cdots,2p \\ \mu_1+\cdots+\mu_{2p}=2}} \left(\prod_{k=1}^{2p} (-\mathrm{eig}_k(\Gamma(\Delta\lambda_{\mathrm{g}i})))^{\mu_k}\right) + \cdots + \\
&\quad \mathrm{Det}(\Gamma(\Delta\lambda_{\mathrm{g}i})) = 0
\end{aligned} \tag{21}$$

Furthermore, denote:

$$\begin{aligned}
&\Psi(\Delta\lambda_{\mathrm{g}i}) = -(s_{\mathrm{g}i} - \lambda_{\mathrm{g}i})^{2p-1}(\mathrm{eig}_1(\Gamma(\Delta\lambda_{\mathrm{g}i})) - \mathrm{tr}(\Gamma(0))) + \\
&\quad (s_{\mathrm{g}i} - \lambda_{\mathrm{g}i})^{2p-1}(-\mathrm{eig}_2(\Gamma(\Delta\lambda_{\mathrm{g}i}))) + \cdots + \\
&\quad (s_{\mathrm{g}i} - \lambda_{\mathrm{g}i})^{2p-1}(-\mathrm{eig}_{2p}(\Gamma(\Delta\lambda_{\mathrm{g}i}))) + (s_{\mathrm{g}i} - \lambda_{\mathrm{g}i})^{2p-2} \times \\
&\quad \sum_{\substack{\mu_k\in\{0,1\} \\ k=1,2,\cdots,2p \\ \mu_1+\cdots+\mu_{2p}=2}} \left(\prod_{k=1}^{2p} (-\mathrm{eig}_k(\Gamma(\Delta\lambda_{\mathrm{g}i})))^{\mu_k}\right) + \cdots + \\
&\quad \mathrm{Det}(\Gamma(\Delta\lambda_{\mathrm{g}i}))
\end{aligned} \tag{22}$$

Then, (21) can be transformed into

$$(s_{\mathrm{g}i} - \lambda_{\mathrm{g}i})^{2p} - (s_{\mathrm{g}i} - \lambda_{\mathrm{g}i})^{2p-1}\mathrm{tr}(\Gamma(0)) + \Psi(\Delta\lambda_{\mathrm{g}i}) = 0 \tag{23}$$

As can be seen, the exact closed-loop SSO mode, $\hat{\lambda}_{\mathrm{g}i}$, is the solution of (20) with $\Delta\lambda_{\mathrm{g}i}$ replaced by $\hat{\lambda}_{\mathrm{g}i} - \lambda_{\mathrm{g}i}$. $\tilde{\hat{\lambda}}_{\mathrm{g}i,r}$ is the solution of $\prod_{k=1}^{2p}(s_{\mathrm{g}i} - \lambda_{\mathrm{g}i} - \mathrm{eig}_k(\Gamma(0))) = 0$.

For obtaining the estimate of $\hat{\lambda}_{\mathrm{g}i}$, rewrite (23) as $F_{\mathrm{g}1}(\alpha,\beta,\nu,\kappa) = 0$ and $F_{\mathrm{g}2}(\alpha,\beta,\nu,\kappa) = 0$, where

$$\begin{aligned}
&F_{\mathrm{g}1}(\alpha,\beta,\nu,\kappa) = \\
&\quad \mathrm{Re}((s_{\mathrm{g}i} - \lambda_{\mathrm{g}i})^{2p} - (s_{\mathrm{g}i} - \lambda_{\mathrm{g}i})^{2p-1}\mathrm{tr}(\Gamma(0)) + \Psi(\Delta\lambda_{\mathrm{g}i})) \\
&F_{\mathrm{g}2}(\alpha,\beta,\nu,\kappa) = \\
&\quad \mathrm{Im}((s_{\mathrm{g}i} - \lambda_{\mathrm{g}i})^{2p} - (s_{\mathrm{g}i} - \lambda_{\mathrm{g}i})^{2p-1}\mathrm{tr}(\Gamma(0)) + \Psi(\Delta\lambda_{\mathrm{g}i}))
\end{aligned} \tag{24}$$

Since $F_{\mathrm{g}1} + \mathrm{j}F_{\mathrm{g}2} = \mathrm{Det}((\nu + j\kappa - \lambda_{\mathrm{g}i})I - \Gamma(\alpha + j\beta))$, when $|\Delta\lambda_{\mathrm{g}i}|$ is small, both $F_{\mathrm{g}1}$ and $F_{\mathrm{g}2}$ are continuously differentiable with respect to ν, κ, α and β. The partial derivatives of $F_{\mathrm{g}1}$ and $F_{\mathrm{g}2}$ with respect to ν and κ are presented as:

$$\begin{aligned}
\frac{\partial F_{\mathrm{g}1}(\alpha,\beta,\nu,\kappa)}{\partial\nu} &= \mathrm{Re}\bigg(\frac{\partial}{\partial\nu}((s_{\mathrm{g}i} - \lambda_{\mathrm{g}i})^{2p} - \\
&\quad (s_{\mathrm{g}i} - \lambda_{\mathrm{g}i})^{2p-1}\mathrm{tr}(\Gamma(0)) + \Psi(\Delta\lambda_{\mathrm{g}i}))\bigg) \\
\frac{\partial F_{\mathrm{g}1}(\alpha,\beta,\nu,\kappa)}{\partial\kappa} &= \mathrm{Re}\bigg(\frac{\partial}{\partial\kappa}((s_{\mathrm{g}i} - \lambda_{\mathrm{g}i})^{2p} - \\
&\quad (s_{\mathrm{g}i} - \lambda_{\mathrm{g}i})^{2p-1}\mathrm{tr}(\Gamma(0)) + \Psi(\Delta\lambda_{\mathrm{g}i}))\bigg) \\
\frac{\partial F_{\mathrm{g}2}(\alpha,\beta,\nu,\kappa)}{\partial\nu} &= \mathrm{Im}\bigg(\frac{\partial}{\partial\nu}((s_{\mathrm{g}i} - \lambda_{\mathrm{g}i})^{2p} - \\
&\quad (s_{\mathrm{g}i} - \lambda_{\mathrm{g}i})^{2p-1}\mathrm{tr}(\Gamma(0)) + \Psi(\Delta\lambda_{\mathrm{g}i}))\bigg) \\
\frac{\partial F_{\mathrm{g}2}(\alpha,\beta,\nu,\kappa)}{\partial\kappa} &= \mathrm{Im}\bigg(\frac{\partial}{\partial\kappa}((s_{\mathrm{g}i} - \lambda_{\mathrm{g}i})^{2p} - \\
&\quad (s_{\mathrm{g}i} - \lambda_{\mathrm{g}i})^{2p-1}\mathrm{tr}(\Gamma(0)) + \Psi(\Delta\lambda_{\mathrm{g}i}))\bigg)
\end{aligned} \tag{25}$$

Via some algebraic manipulations, it can be proved that

$$\begin{aligned}
\left.\frac{\partial F_{\mathrm{g}1}}{\partial\nu}\right|_{\substack{\alpha+\mathrm{j}\beta=0 \\ \nu+\mathrm{j}\kappa=s_{\mathrm{g}i}^0}} &= \mathrm{Re}(2p(s_{\mathrm{g}i}^0 - \lambda_{\mathrm{g}i})^{2p-1} - \\
&\quad (2p-1)(s_{\mathrm{g}i}^0 - \lambda_{\mathrm{g}i})^{2p-2}\mathrm{tr}(\Gamma(0))) \\
\left.\frac{\partial F_{\mathrm{g}2}}{\partial\nu}\right|_{\substack{\alpha+\mathrm{j}\beta=0 \\ \nu+\mathrm{j}\kappa=s_{\mathrm{g}i}^0}} &= \mathrm{Im}(2p(s_{\mathrm{g}i}^0 - \lambda_{\mathrm{g}i})^{2p-1} - \\
&\quad (2p-1)(s_{\mathrm{g}i}^0 - \lambda_{\mathrm{g}i})^{2p-2}\mathrm{tr}(\Gamma(0))) \\
\left.\frac{\partial F_{\mathrm{g}1}}{\partial\kappa}\right|_{\substack{\alpha+\mathrm{j}\beta=0 \\ \nu+\mathrm{j}\kappa=s_{\mathrm{g}i}^0}} &= \mathrm{Re}(\mathrm{j}2p(s_{\mathrm{g}i}^0 - \lambda_{\mathrm{g}i})^{2p-1} - \\
&\quad \mathrm{j}(2p-1)(s_{\mathrm{g}i}^0 - \lambda_{\mathrm{g}i})^{2p-2}\mathrm{tr}(\Gamma(0))) \\
\left.\frac{\partial F_{\mathrm{g}2}}{\partial\kappa}\right|_{\substack{\alpha+\mathrm{j}\beta=0 \\ \nu+\mathrm{j}\kappa=s_{\mathrm{g}i}^0}} &= \mathrm{Im}(\mathrm{j}2p(s_{\mathrm{g}i}^0 - \lambda_{\mathrm{g}i})^{2p-1} -
\end{aligned}$$

$$\mathrm{j}(2p-1)(s_{\mathrm{g}i}^0-\lambda_{\mathrm{g}i})^{2p-2}\mathrm{tr}(\Gamma(0))) \quad (26)$$

where $s_{\mathrm{g}i}^0=\tilde{\hat{\lambda}}_{\mathrm{g}i,r}$. For $\frac{\partial F_{\mathrm{g}1}}{\partial \alpha}$, $\frac{\partial F_{\mathrm{g}1}}{\partial \beta}$, $\frac{\partial F_{\mathrm{g}2}}{\partial \alpha}$ and $\frac{\partial F_{\mathrm{g}2}}{\partial \beta}$, they can be expressed as:

$$\begin{aligned}\frac{\partial F_{\mathrm{g}1}}{\partial \alpha}&=\mathrm{Re}\left(\frac{\partial}{\partial \alpha}\mathrm{Det}((\nu+\mathrm{j}\kappa-\lambda_{\mathrm{g}i})I-\Gamma(\alpha+\mathrm{j}\beta))\right)\\ \frac{\partial F_{\mathrm{g}1}}{\partial \beta}&=\mathrm{Re}\left(\frac{\partial}{\partial \beta}\mathrm{Det}((\nu+\mathrm{j}\kappa-\lambda_{\mathrm{g}i})I-\Gamma(\alpha+\mathrm{j}\beta))\right)\\ \frac{\partial F_{\mathrm{g}2}}{\partial \alpha}&=\mathrm{Im}\left(\frac{\partial}{\partial \alpha}\mathrm{Det}((\nu+\mathrm{j}\kappa-\lambda_{\mathrm{g}i})I-\Gamma(\alpha+\mathrm{j}\beta))\right)\\ \frac{\partial \mathrm{F}_{g2}}{\partial \beta}&=\mathrm{Im}\left(\frac{\partial}{\partial \beta}\mathrm{Det}((\nu+\mathrm{j}\kappa-\lambda_{\mathrm{g}i})I-\Gamma(\alpha+\mathrm{j}\beta))\right) \quad (27)\end{aligned}$$

Based on the idea of fixed-point iteration [22], [23] and implicit function theorem [24], [25], the estimate of $\hat{\lambda}_{\mathrm{g}i}$ is given as:

$$\begin{aligned}&\begin{bmatrix}\mathrm{Re}(\hat{\lambda}_{\mathrm{g}i,\mathrm{est}})\\ \mathrm{Im}(\hat{\lambda}_{\mathrm{g}i,\mathrm{est}})\end{bmatrix}=\\ &\begin{bmatrix}\mathrm{Re}(\tilde{\hat{\lambda}}_{\mathrm{g}i,r})\\ \mathrm{Im}(\tilde{\hat{\lambda}}_{\mathrm{g}i,r})\end{bmatrix}-\left(\left.\begin{bmatrix}\frac{\partial F_{\mathrm{g}1}}{\partial \nu} & \frac{\partial F_{\mathrm{g}1}}{\partial \kappa}\\ \frac{\partial F_{\mathrm{g}2}}{\partial \nu} & \frac{\partial F_{\mathrm{g}2}}{\partial \kappa}\end{bmatrix}\right|_{\substack{\alpha+\mathrm{j}\beta=0\\ \nu+\mathrm{j}\kappa=s_{\mathrm{g}i}^0}}\right)^{-1}\\ &\cdot\left(\left.\begin{bmatrix}\frac{\partial F_{\mathrm{g}1}}{\partial \alpha} & \frac{\partial F_{\mathrm{g}1}}{\partial \beta}\\ \frac{\partial F_{\mathrm{g}2}}{\partial \alpha} & \frac{\partial F_{\mathrm{g}2}}{\partial \beta}\end{bmatrix}\right|_{\substack{\alpha+\mathrm{j}\beta=0\\ \nu+\mathrm{j}\kappa=s_{\mathrm{g}i}^0}}\right)\begin{bmatrix}\mathrm{Re}(\Delta\lambda_{\mathrm{g}i})\\ \mathrm{Im}(\Delta\lambda_{\mathrm{g}i})\end{bmatrix} \quad (28)\end{aligned}$$

where $\hat{\lambda}_{\mathrm{g}i,\mathrm{est}}$ is the estimate of $\hat{\lambda}_{\mathrm{g}i}$, and $-\begin{bmatrix}\frac{\partial F_{\mathrm{g}1}}{\partial \nu} & \frac{\partial F_{\mathrm{g}1}}{\partial \kappa}\\ \frac{\partial F_{\mathrm{g}2}}{\partial \nu} & \frac{\partial F_{\mathrm{g}2}}{\partial \kappa}\end{bmatrix}^{-1}\begin{bmatrix}\frac{\partial F_{\mathrm{g}1}}{\partial \alpha} & \frac{\partial F_{\mathrm{g}1}}{\partial \beta}\\ \frac{\partial F_{\mathrm{g}2}}{\partial \alpha} & \frac{\partial F_{\mathrm{g}2}}{\partial \beta}\end{bmatrix}$ is interpreted as the partial derivatives of (ν,κ) with respect to (α,β), according to the implicit function theorem [26], [27].

Besides, for estimation of $\hat{\lambda}_{\mathrm{w}h,i}$, denote

$$\begin{aligned}&\Delta\lambda_{\mathrm{w}h,i}=s-\lambda_{\mathrm{w}h,i}=\omega+\mathrm{j}\zeta \quad s_{\mathrm{w}h,i}=\mu+\mathrm{j}\varphi\\ &\Gamma(\Delta\lambda_{\mathrm{w}h,i})=\left(\sum_{j=1}^{n_{\mathrm{g}}}\frac{R_{\mathrm{g}j}}{\Delta\lambda_{\mathrm{w}h,i}+\lambda_{\mathrm{w}h,i}-\lambda_{\mathrm{g}j}}\right)\\ &\left(R_{\mathrm{w}h,i}+\sum_{j=1,j\neq i}^{n_{\mathrm{w}h}}\frac{R_{\mathrm{w}h,j}\cdot\Delta\lambda_{\mathrm{w}h,i}}{\Delta\lambda_{\mathrm{w}h,i}+\lambda_{\mathrm{w}h,i}-\lambda_{\mathrm{w}h,j}}+\right.\\ &\left.\sum_{l=1,l\neq h}^{\mathrm{p}}\frac{R_{\mathrm{w}l,j}\cdot\Delta\lambda_{\mathrm{w}h,i}}{\Delta\lambda_{\mathrm{w}h,i}+\lambda_{\mathrm{w}h,i}-\lambda_{\mathrm{w}l,j}}\right)\end{aligned}$$

Obviously, equation $\mathrm{Det}((s_{\mathrm{w}h,i}-\lambda_{\mathrm{w}h,i})I-\Gamma(\Delta\lambda_{\mathrm{w}h,i}))=0$ is equivalent to

$$\prod_{k=1}^{2p}(s_{\mathrm{w}h,i}-\lambda_{\mathrm{w}h,i}-\mathrm{eig}_k(\Gamma(\Delta\lambda_{\mathrm{w}h,i})))=0 \quad (29)$$

Similar to derivations from (21) to (24), (29) can be expressed as $F_{\mathrm{d}1}(\omega,\zeta,\mu,\varphi)=0$ and $F_{\mathrm{d}2}(\omega,\zeta,\mu,\varphi)=0$, where

$$\begin{aligned}&F_{\mathrm{d}1}(\omega,\zeta,\mu,\varphi)\\ &=\mathrm{Re}((s_{\mathrm{w}h,i}-\lambda_{\mathrm{w}h,i})^{2p}-\\ &\quad(s_{\mathrm{w}h,i}-\lambda_{\mathrm{w}h,i})^{2p-1}\mathrm{tr}(\Gamma(0))+\Psi(\Delta\lambda_{\mathrm{w}h,i}))\end{aligned}$$

$$\begin{aligned}&F_{\mathrm{d}2}(\omega,\zeta,\mu,\varphi)\\ &=\mathrm{Im}((s_{\mathrm{w}h,i}-\lambda_{\mathrm{w}h,i})^{2p}-\\ &\quad(s_{\mathrm{w}h,i}-\lambda_{\mathrm{w}h,i})^{2p-1}\mathrm{tr}(\Gamma(0))+\Psi(\Delta\lambda_{\mathrm{w}h,i})) \quad (30)\end{aligned}$$

Moreover, similar to $F_{\mathrm{g}1}$ and $F_{\mathrm{g}2}$, when $|\Delta\lambda_{\mathrm{w}h,i}|$ is small, both $F_{\mathrm{d}1}$ and $F_{\mathrm{d}2}$ are continuously differentiable with respect to μ, φ, ω and ζ. Finally, based on the idea of fixed-point iteration and implicit function theorem, estimate of $\hat{\lambda}_{\mathrm{w}h,i}$ is given as:

$$\begin{aligned}&\begin{bmatrix}\mathrm{Re}(\hat{\lambda}_{\mathrm{w}h,i,\mathrm{est}})\\ \mathrm{Im}(\hat{\lambda}_{\mathrm{w}h,i,\mathrm{est}})\end{bmatrix}=\\ &\begin{bmatrix}\mathrm{Re}(\tilde{\hat{\lambda}}_{\mathrm{w}h,i,r})\\ \mathrm{Im}(\tilde{\hat{\lambda}}_{\mathrm{w}h,i,r})\end{bmatrix}-\left(\left.\begin{bmatrix}\frac{\partial F_{\mathrm{d}1}}{\partial \mu} & \frac{\partial F_{\mathrm{d}1}}{\partial \varphi}\\ \frac{\partial F_{\mathrm{d}2}}{\partial \mu} & \frac{\partial F_{\mathrm{d}2}}{\partial \varphi}\end{bmatrix}\right|_{\substack{\mu+j\varphi=\tilde{\hat{\lambda}}_{\mathrm{w}h,i,r}\\ \omega+j\zeta=0}}\right)^{-1}\\ &\cdot\left(\left.\begin{bmatrix}\frac{\partial F_{\mathrm{d}1}}{\partial \omega} & \frac{\partial F_{\mathrm{d}1}}{\partial \zeta}\\ \frac{\partial F_{\mathrm{d}2}}{\partial \omega} & \frac{\partial F_{\mathrm{d}2}}{\partial \zeta}\end{bmatrix}\right|_{\substack{\mu+j\varphi=\tilde{\hat{\lambda}}_{\mathrm{w}h,i,r}\\ \omega+j\zeta=0}}\right)\begin{bmatrix}\mathrm{Re}(\Delta\lambda_{\mathrm{w}hi})\\ \mathrm{Im}(\Delta\lambda_{\mathrm{w}hi})\end{bmatrix} \quad (31)\end{aligned}$$

where $\hat{\lambda}_{\mathrm{w}h,i,\mathrm{est}}$ is the estimate of $\hat{\lambda}_{\mathrm{w}h,i}$, and $-\begin{bmatrix}\frac{\partial F_{\mathrm{d}1}}{\partial \mu} & \frac{\partial F_{\mathrm{d}1}}{\partial \varphi}\\ \frac{\partial F_{\mathrm{d}2}}{\partial \mu} & \frac{\partial F_{\mathrm{d}2}}{\partial \varphi}\end{bmatrix}^{-1}\begin{bmatrix}\frac{\partial F_{\mathrm{d}1}}{\partial \omega} & \frac{\partial F_{\mathrm{d}1}}{\partial \zeta}\\ \frac{\partial F_{\mathrm{d}2}}{\partial \omega} & \frac{\partial F_{\mathrm{d}2}}{\partial \zeta}\end{bmatrix}$ is interpreted as the partial derivatives of (μ,φ) with respect to (ω,ζ), according to the implicit function theorem.

Remark 1. In practice, $\hat{\lambda}_{\mathrm{w}h,i,\mathrm{est}}$ and $\hat{\lambda}_{\mathrm{g},i,\mathrm{est}}$ can be calculated based on the identified parameters of DFIG subsystem.

III. Study Cases

In this section, a study case is presented to verify accuracy of the parameter identification method and demonstrate the mechanism of asymmetric SSR and features of the proposed SSR detection method. This case is performed in the 4-machine 11-bus power system with two DFIG-WFs integrated. Existence of ASSMA and ASSMR in this system, affected by variation of k_{dcp} and k_{dci}, will be demonstrated. k_{dcp} and k_{dci} are the proportional gain and integral gain of the PI controller in DC-link voltage control loop.

Figure 4 shows the structure of the 4-machine 11-bus power system. In the system, the 1st DFIG-WF(DFIG1) is connected at bus 12, while the 2nd DFIG-WF(DFIG2) is connected at bus 13. both DFIG1 and DFIG2 are comprised of 50 DFIG-WTs. The detailed 19th-order model of the DFIG-WT, including its control systems, is given in [28]. Besides, models and parameters of transmission lines, transformers and loads are obtained from [21]. Models and parameters of the four SGs are given in [29]. Note the six-mass model is adopted for modeling the shaft system of SG.

Since the parameters of DFIG1 are necessary for detecting ASSMA and ASSMR, reinforcement learning and least square method are used to identify them in this study case. The K_{tg} of DFIG1, denoted as $K_{\mathrm{tg}1}$, is identified via reinforcement learning. The identified result of $K_{\mathrm{tg}1}$, denoted as $\tilde{K}_{\mathrm{tg}1}$, is 498.2457, while actual value of $K_{\mathrm{tg}1}$ is 500. Besides, $T_{\mathrm{g}1}$, as well as its estimate $\tilde{T}_{\mathrm{g}1}$, are shown in Fig. 5. Remaining parameters of DFIG1, including $R_{\mathrm{s}}, L_{\mathrm{s}}, R_{\mathrm{r}}, L_{\mathrm{r}}, L_{\mathrm{m}}, R_{\mathrm{c}}, L_{\mathrm{c}}, C, H_{\mathrm{g}}$, $H_{\mathrm{t}}, D_{\mathrm{t}}, D_{\mathrm{g}}$ and D_{tg} are estimated by least squares method.

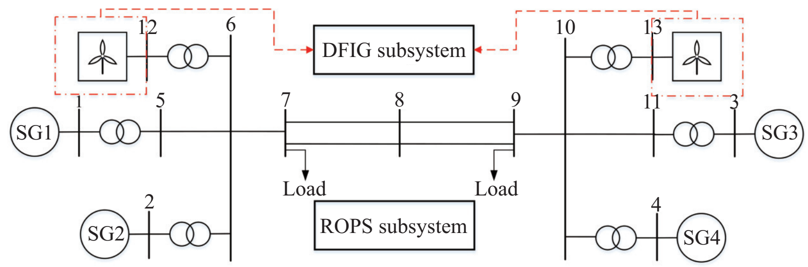

Fig. 4. Configuration of the 4-machine 11-bus power system.

Estimated values and actual values of those parameters are listed in Table I.

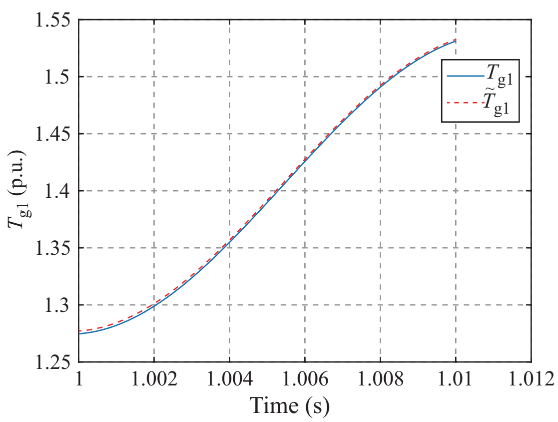

Fig. 5. Comparison between $T_{\rm g1}$ and its estimate $\tilde{T}_{\rm g1}$.

TABLE I
PARAMETERS OF DFIG

Name	Identified value	Actual value
$\tilde{R}_{\rm s}$ (p.u.)	4.8219×10^{-4}	0.1×10^{-4}
$\tilde{L}_{\rm s}$ (p.u.)	5.7892	5.8333
$\tilde{R}_{\rm r}$ (p.u.)	6.7275×10^{-4}	0.1×10^{-4}
$\tilde{L}_{\rm r}$ (p.u.)	5.789	5.8333
$\tilde{L}_{\rm m}$ (p.u.)	4.9619	5
$\tilde{R}_{\rm c}$ (Ω)	7.877×10^{-8}	0.1×10^{-4}
$\tilde{L}_{\rm c}$ (H)	0.2375	0.2375
$\tilde{C}$ (F)	0.0376	0.0376
$\tilde{H}_{\rm g}$ (s)	1.7936	1.8
$\tilde{H}_{\rm t}$ (s)	4.2696	4.29
$\tilde{D}_{\rm t}$ (p.u.)	0.0083	0.01
$\tilde{D}_{\rm g}$ (p.u.)	0.0083	0.01
$\tilde{D}_{\rm tg}$ (p.u.)	2.9748	3

The example power system is divided into DFIG subsystem and ROPS subsystem. As for the ROPS subsystem, the eigenvalue of $A_{\rm r}$ corresponding to the open-loop speed mode(SM) of SG is of great concern as it is sufficiently close to the imaginary axis of the complex plane, under a wide range of operating conditions and system parameters [8]. Moreover, it is possible for the SM to interact with one or more modes of DFIG subsystem, resulting in ASSMA or ASSMR. What's worse, if ASSMR happens, the small-signal stability of the entire power system may be lost [8]. In this study case, the eigenvalue corresponding to the open-loop SM of the 3rd mass of the shaft system of SG2(ω_3), denoted as $\lambda_{\rm r3-2}$, is $-0.1348+{\rm j}95.5069$, while the eigenvalue corresponding to the open-loop SM of the 4th mass of the shaft system of SG2(ω_4), denoted as $\lambda_{\rm r4-2}$, is $-0.14851 + {\rm j}130.78$. Both $\lambda_{\rm r3-2}$ and $\lambda_{\rm r4-2}$ are forced to interact with the eigenvalue of $A_{\rm d}$ corresponding to the open-loop DC-link voltage mode(DCLVM) of DFIG1, denoted as $\lambda_{\rm dc}$, to study ASSMA and ASSMR.

In order to verify existence of ASSMA and ASSMR originated from interaction between $\lambda_{\rm r3-2}$, $\lambda_{\rm r4-2}$ and $\lambda_{\rm dc}$, $k_{\rm dcp}$ and $k_{\rm dci}$ are varied from $k_{\rm dcp} = 0.1$, $k_{\rm dci} = 250$ to $k_{\rm dcp} = 0.35$, $k_{\rm dci} = 800$. It is worth noting variation of $k_{\rm dcp}$ and $k_{\rm dci}$ brings no impact on the operating condition of ROPS subsystem. In addition, locations of $\hat{\lambda}_{\rm r3-2}$ for $k_{\rm dcp} = 0.1475$, $k_{\rm dci} = 331.21475$ and $k_{\rm dcp} = 0.1502$, $k_{\rm dci} = 338.0282$, locations of $\hat{\lambda}_{\rm r4-2}$ for $k_{\rm dcp} = 0.2711$, $k_{\rm dci} = 618.4881$ and $k_{\rm dcp} = 0.2783$, $k_{\rm dci} = 636.6573$, as well as locations of $\hat{\lambda}_{\rm dc}$ for $k_{\rm dcp} = 0.1475$, $k_{\rm dci} = 331.21475$, $k_{\rm dcp} = 0.1502$, $k_{\rm dci} = 338.0282$, $k_{\rm dcp} = 0.2711$, $k_{\rm dci} = 618.4881$ and $k_{\rm dcp} = 0.2783$, $k_{\rm dci} = 636.6573$, are estimated by the proposed method. Note $\hat{\lambda}_{\rm r3-2}, \hat{\lambda}_{\rm r4-2}$ and $\hat{\lambda}_{\rm dc}$ are the closed-loop SSO modes corresponding to $\lambda_{\rm r3-2}$, $\lambda_{\rm r4-2}$ and $\lambda_{\rm dc}$ respectively.

Figure 6 displays the location of $\lambda_{\rm r3-2}$ and the trajectories of $\hat{\lambda}_{\rm r3-2}$, $\lambda_{\rm dc}$ and $\hat{\lambda}_{\rm dc}$ as $k_{\rm dcp}$, $k_{\rm dci}$ increase from $k_{\rm dcp} = 0.1$, $k_{\rm dci} = 250$ to $k_{\rm dcp} = 0.2$, $k_{\rm dci} = 400$. As is presented, ${\rm Re}(\lambda_{\rm r3-2}) > {\rm Re}(\lambda_{\rm dc})$ for all $k_{\rm dcp} \in [0.1, 0.2]$ and $k_{\rm dci} \in [250, 400]$. In addition, with $k_{\rm dci}$ increasing from 250 to 336 and $k_{\rm dcp}$ from 0.1 to 0.148, $|\lambda_{\rm r3-2} - \lambda_{\rm dc}|$ arrives at a local minimum when $k_{\rm dcp} = 0.1475$, $k_{\rm dci} = 331.21475$. Because ${\rm Re}(\Delta\lambda_{\rm r3-2}) = \hat{\lambda}_{\rm r3-2} - \lambda_{\rm r3-2} = 0.1257 > 0$ when $k_{\rm dcp} = 0.1475$, $k_{\rm dci} = 331.21475$, as indicated from Table II, ASSMR happens in the 4-machine 11-bus power system as $k_{\rm dcp}$ and $k_{\rm dci}$ vary from $k_{\rm dcp} = 0.1$, $k_{\rm dci} = 250$ to $k_{\rm dcp} = 0.148$, $k_{\rm dci} = 336$. What's more, as $k_{\rm dcp}$, $k_{\rm dci}$ increases further from $k_{\rm dcp} = 0.148$, $k_{\rm dci} = 336$ to $k_{\rm dcp} = 0.2$, $k_{\rm dci} = 400$, $|\lambda_{\rm r3-2} - \lambda_{\rm dc}|$ arrives at a new local minimum when $k_{\rm dcp} = 0.1502$, $k_{\rm dci} = 338.0282$. Due to the fact that ${\rm Re}(\Delta\lambda_{\rm r3-2}) = -0.2058 < 0$ when $k_{\rm dcp} = 0.1502$, $k_{\rm dci} = 338.0282$, ASSMA occurs in the power system when $k_{\rm dcp}$ and $k_{\rm dci}$ are tuned from $k_{\rm dcp} = 0.148$, $k_{\rm dci} = 336$ to $k_{\rm dcp} = 0.2$, $k_{\rm dci} = 400$. Besides, estimates of $\hat{\lambda}_{\rm r3-2}$ and $\hat{\lambda}_{\rm dc}$ given by the proposed method using actual system parameters, denoted as $\tilde{\hat{\lambda}}_{\rm r3-2}$ and $\tilde{\hat{\lambda}}_{\rm dc}$ respectively, estimates of $\hat{\lambda}_{\rm r3-2}$ and $\hat{\lambda}_{\rm dc}$ given by the proposed method using the identified system parameters, denoted as $\tilde{\hat{\lambda}}^{\rm s2}_{\rm r3-2}$ and $\tilde{\hat{\lambda}}^{\rm s2}_{\rm dc}$ are demonstrated in Fig. 6. Besides, estimates of $\hat{\lambda}_{\rm r3-2}$ and $\hat{\lambda}_{\rm dc}$ given by the method proposed in [1], denoted as $\tilde{\hat{\lambda}}^{\rm o}_{\rm r3-2}$ and $\tilde{\hat{\lambda}}^{\rm o}_{\rm dc}$, as well as

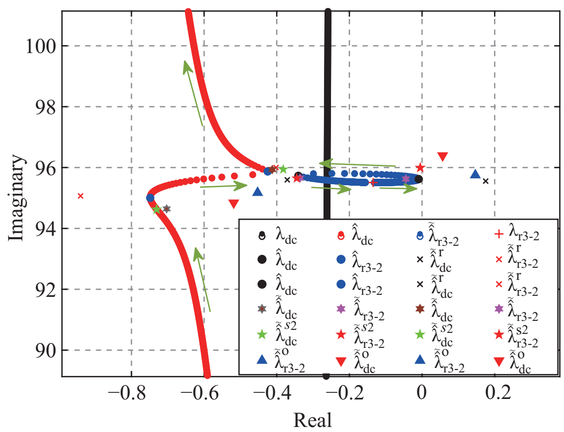

Fig. 6. Trajectories of eigenvalues and their estimates as k_{dcp} and k_{dci} increase from $k_{\mathrm{dcp}} = 0.1$, $k_{\mathrm{dci}} = 250$ to $k_{\mathrm{dcp}} = 0.2$, $k_{\mathrm{dci}} = 400$.

TABLE II
THE ACTUAL AND ESTIMATED LOCATIONS OF $\hat{\lambda}_{\mathrm{r}3-2}$ AND $\hat{\lambda}_{\mathrm{dc}}$

	$k_{\mathrm{dcp}} = 0.1475$ $k_{\mathrm{dci}} = 331.21475$	$k_{\mathrm{dcp}} = 0.1502$ $k_{\mathrm{dci}} = 338.0282$
$\hat{\lambda}_{\mathrm{r}3-2}$	−0.0091+j95.6203	−0.3406+j95.7280
$\tilde{\hat{\lambda}}_{\mathrm{r}3-2}$	−0.0445+j95.6254	−0.3357+j95.6569
$\tilde{\hat{\lambda}}^{\mathrm{o}}_{\mathrm{r}3-2}$	0.1466+j95.7509	−0.4527+j95.1730
$\tilde{\hat{\lambda}}^{\mathrm{r}}_{\mathrm{r}3-2}$	0.1752+j95.5547	−0.3710+j95.5967
$\tilde{\hat{\lambda}}^{\mathrm{s2}}_{\mathrm{r}3-2}$	−0.00482+j95.9961	−0.3451+j95.6479
$\hat{\lambda}_{\mathrm{dc}}$	−0.7484+j95.0048	−0.4249+j95.8715
$\tilde{\hat{\lambda}}_{\mathrm{dc}}$	−0.7031+j94.6422	−0.4122+j95.9351
$\tilde{\hat{\lambda}}^{\mathrm{o}}_{\mathrm{dc}}$	−0.5430+j94.8439	0.0567+j96.3953
$\tilde{\hat{\lambda}}^{\mathrm{r}}_{\mathrm{dc}}$	−0.9401+j95.0675	−0.4020+j96
$\tilde{\hat{\lambda}}^{\mathrm{s2}}_{\mathrm{dc}}$	−0.730887+j94.6253	−0.3821+j95.9416

the estimates of $\hat{\lambda}_{\mathrm{r}3-2}$ and $\hat{\lambda}_{\mathrm{dc}}$ given by the method proposed in [8], denoted as $\tilde{\hat{\lambda}}^{\mathrm{r}}_{\mathrm{r}3-2}$ and $\tilde{\hat{\lambda}}^{\mathrm{r}}_{\mathrm{dc}}$, are also presented in Fig. 6. In particular, values of $\tilde{\hat{\lambda}}_{\mathrm{r}3-2}$, $\tilde{\hat{\lambda}}_{\mathrm{dc}}$, $\tilde{\hat{\lambda}}^{\mathrm{s2}}_{\mathrm{r}3-2}$, $\tilde{\hat{\lambda}}^{\mathrm{s2}}_{\mathrm{dc}}$, $\tilde{\hat{\lambda}}^{\mathrm{o}}_{\mathrm{r}3-2}$, $\tilde{\hat{\lambda}}^{\mathrm{o}}_{\mathrm{dc}}$, $\tilde{\hat{\lambda}}^{\mathrm{r}}_{\mathrm{r}3-2}$ and $\tilde{\hat{\lambda}}^{\mathrm{r}}_{\mathrm{dc}}$ for $k_{\mathrm{dcp}} = 0.1475$, $k_{\mathrm{dci}} = 331.21475$ and $k_{\mathrm{dcp}} = 0.1502$, $k_{\mathrm{dci}} = 338.0282$ are listed in Table II. It can be confirmed from Fig. 6 and Table II that compared to $\tilde{\hat{\lambda}}^{\mathrm{o}}_{\mathrm{r}3-2}$ and $\tilde{\hat{\lambda}}^{\mathrm{r}}_{\mathrm{r}3-2}$, $\tilde{\hat{\lambda}}_{\mathrm{r}3-2}$ is closer to $\hat{\lambda}_{\mathrm{r}3-2}$. Besides, since $\tilde{\hat{\lambda}}_{\mathrm{r}3-2}$ is also close to $\tilde{\hat{\lambda}}^{\mathrm{s2}}_{\mathrm{r}3-2}$, accuracy of parameter identification is relatively high, which guarantees adaptability of the proposed open-loop analysis method to parameter uncertainty.

Figure 7 demonstrates location of $\lambda_{\mathrm{r}4-2}$, as well as trajectories of $\hat{\lambda}_{\mathrm{r}4-2}$, $\hat{\lambda}_{\mathrm{dc}}$ and λ_{dc} with both k_{dcp} and k_{dci} increasing from $k_{\mathrm{dcp}} = 0.2$, $k_{\mathrm{dci}} = 400$ to $k_{\mathrm{dcp}} = 0.35$, $k_{\mathrm{dci}} = 800$. As is presented, $\mathrm{Re}(\lambda_{\mathrm{r}4-2}) > \mathrm{Re}(\lambda_{\mathrm{dc}})$ for all $k_{\mathrm{dcp}} \in [0.2, 0.35]$ and all $k_{\mathrm{dci}} \in [400{,}800]$. In addition, when $k_{\mathrm{dcp}} = 0.2711$, $k_{\mathrm{dci}} = 618.4881$, $|\lambda_{\mathrm{r}4-2} - \lambda_{\mathrm{dc}}|$ reaches a local minimum. Because $\mathrm{Re}(\Delta\lambda_{\mathrm{r}4-2}) = 0.1529333 > 0$ for $k_{\mathrm{dcp}} = 0.2711$, $k_{\mathrm{dci}} = 618.4881$, as can be deduced from Table III, ASSMR arises in the power system, with k_{dcp} and k_{dci} tuned from 0.2, 400 to 0.25, 625. Moreover, as k_{dcp}, k_{dci} increase further from $k_{\mathrm{dcp}} = 0.25$, $k_{\mathrm{dci}} = 625$ to $k_{\mathrm{dcp}} = 0.35$, $k_{\mathrm{dci}} = 800$, $|\lambda_{\mathrm{r}4-2} - \lambda_{\mathrm{dc}}|$ arrives at a new local minimum when $k_{\mathrm{dcp}} = 0.2783$, $k_{\mathrm{dci}} = 636.6573$.

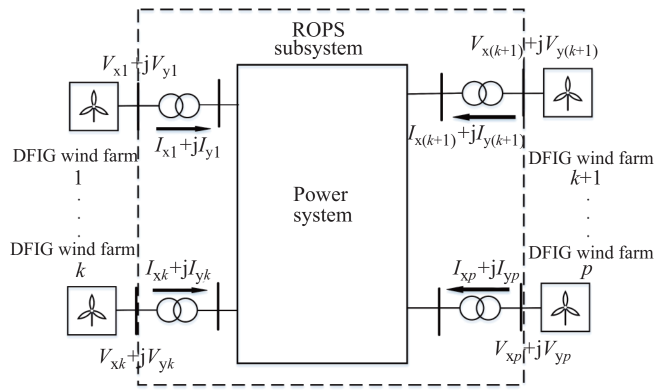

Fig. 7. Trajectories of eigenvalues and their estimates as k_{dcp} and k_{dci} increase from $k_{\mathrm{dcp}} = 0.2$, $k_{\mathrm{dci}} = 400$ to $k_{\mathrm{dcp}} = 0.35$, $k_{\mathrm{dci}} = 800$.

TABLE III
THE ACTUAL AND ESTIMATED LOCATIONS OF $\hat{\lambda}_{\mathrm{r}4-2}$ AND $\hat{\lambda}_{\mathrm{dc}}$

	$k_{\mathrm{dcp}} = 0.2711$ $k_{\mathrm{dci}} = 618.4881$	$k_{\mathrm{dcp}} = 0.2783$ $k_{\mathrm{dci}} = 636.6573$
$\hat{\lambda}_{\mathrm{r}4-2}$	0.00442+j130.91	−0.2955+j130.96
$\tilde{\hat{\lambda}}_{\mathrm{r}4-2}$	0.0526+j131.2029	−0.3118+j130.9412
$\tilde{\hat{\lambda}}^{\mathrm{o}}_{\mathrm{r}4-2}$	0.26458+j131.12	−0.5692+j130.43
$\tilde{\hat{\lambda}}^{\mathrm{r}}_{\mathrm{r}4-2}$	0.1874+j130.81	−0.3978+j130.88
$\tilde{\hat{\lambda}}^{\mathrm{s2}}_{\mathrm{r}4-2}$	0.07+j131.2037	−0.3157+j130.9395
$\hat{\lambda}_{\mathrm{dc}}$	−1.2347+j129.96	−0.9560+j131.74
$\tilde{\hat{\lambda}}_{\mathrm{dc}}$	−1.215+j129.7429	−0.9214+j131.7417
$\tilde{\hat{\lambda}}^{\mathrm{o}}_{\mathrm{dc}}$	−0.78971+j129.63	0.045292+j132.21
$\tilde{\hat{\lambda}}^{\mathrm{r}}_{\mathrm{dc}}$	−1.4293+j130.02	−0.8662+j131.84
$\tilde{\hat{\lambda}}^{\mathrm{s2}}_{\mathrm{dc}}$	−1.2013+j129.7333	−0.8946+j131.7386

Since $\mathrm{Re}(\Delta\lambda_{\mathrm{r}4-2}) = -0.14695 < 0$ when $k_{\mathrm{dcp}} = 0.2783$, $k_{\mathrm{dci}} = 636.6573$, ASSMA occurs in the power system when k_{dcp} and k_{dci} are tuned from $k_{\mathrm{dcp}} = 0.25$, $k_{\mathrm{dci}} = 625$ to $k_{\mathrm{dcp}} = 0.35$, $k_{\mathrm{dci}} = 800$. Besides, estimates of $\hat{\lambda}_{\mathrm{r}4-2}$ and $\hat{\lambda}_{\mathrm{dc}}$ given by the proposed method using actual system parameters, denoted as $\tilde{\hat{\lambda}}_{\mathrm{r}4-2}$ and $\tilde{\hat{\lambda}}_{\mathrm{dc}}$ respectively, estimates of $\hat{\lambda}_{\mathrm{r}4-2}$ and $\hat{\lambda}_{\mathrm{dc}}$ given by the proposed method using identified system parameters, denoted as $\tilde{\hat{\lambda}}^{\mathrm{s2}}_{\mathrm{r}4-2}$ and $\tilde{\hat{\lambda}}^{\mathrm{s2}}_{\mathrm{dc}}$, are displayed in Fig. 7. Moreover, estimates of $\hat{\lambda}_{\mathrm{r}4-2}$ and $\hat{\lambda}_{\mathrm{dc}}$ given by the method proposed in [1], denoted as $\tilde{\hat{\lambda}}^{\mathrm{o}}_{\mathrm{r}4-2}$ and $\tilde{\hat{\lambda}}^{\mathrm{o}}_{\mathrm{dc}}$, as well as estimates of $\hat{\lambda}_{\mathrm{r}4-2}$ and $\hat{\lambda}_{\mathrm{dc}}$ given by the method proposed in [8], denoted as $\tilde{\hat{\lambda}}^{\mathrm{r}}_{\mathrm{r}4-2}$ and $\tilde{\hat{\lambda}}^{\mathrm{r}}_{\mathrm{dc}}$, are demonstrated in Fig. 7. In particular, the values of $\tilde{\hat{\lambda}}_{\mathrm{r}4-2}$, $\tilde{\hat{\lambda}}_{\mathrm{dc}}$, $\tilde{\hat{\lambda}}^{\mathrm{s2}}_{\mathrm{r}4-2}$, $\tilde{\hat{\lambda}}^{\mathrm{s2}}_{\mathrm{dc}}$, $\tilde{\hat{\lambda}}^{\mathrm{o}}_{\mathrm{r}4-2}$, $\tilde{\hat{\lambda}}^{\mathrm{o}}_{\mathrm{dc}}$, $\tilde{\hat{\lambda}}^{\mathrm{r}}_{\mathrm{r}4-2}$ and $\tilde{\hat{\lambda}}^{\mathrm{r}}_{\mathrm{dc}}$ for $k_{\mathrm{dcp}} = 0.2711$, $k_{\mathrm{dci}} = 618.4881$ and $k_{\mathrm{dcp}} = 0.2783$, $k_{\mathrm{dci}} = 636.6573$ are listed in Table III. It can be confirmed from Fig. 7 and Table III that compared to $\tilde{\hat{\lambda}}^{\mathrm{o}}_{\mathrm{r}4-2}$ and $\tilde{\hat{\lambda}}^{\mathrm{r}}_{\mathrm{r}4-2}$, $\tilde{\hat{\lambda}}_{\mathrm{r}4-2}$ is closer to $\hat{\lambda}_{\mathrm{r}4-2}$. $\tilde{\hat{\lambda}}^{\mathrm{s2}}_{\mathrm{r}4-2}$ is also close to $\tilde{\hat{\lambda}}_{\mathrm{r}4-2}$.

To confirm existence of ASSMA and ASSMR in different ways, time domain simulation is carried out on the 4-machine 11-bus power system. Simulation results are shown in Fig. 8. According to Fig. 8(a) and (b), decay time constant and frequency of ω_3 and U_{dc} are matched with those indicated by the real and imaginary part of $\hat{\lambda}_{\mathrm{r}3-2}$ and $\hat{\lambda}_{\mathrm{dc}}$ for $k_{\mathrm{dcp}} = 0.1475, k_{\mathrm{dci}} = 331.21475$ and $k_{\mathrm{dcp}} = 0.1502, k_{\mathrm{dci}} = 338.0282$. Similarly, Fig. 8(c) and (d) reflect the decay time

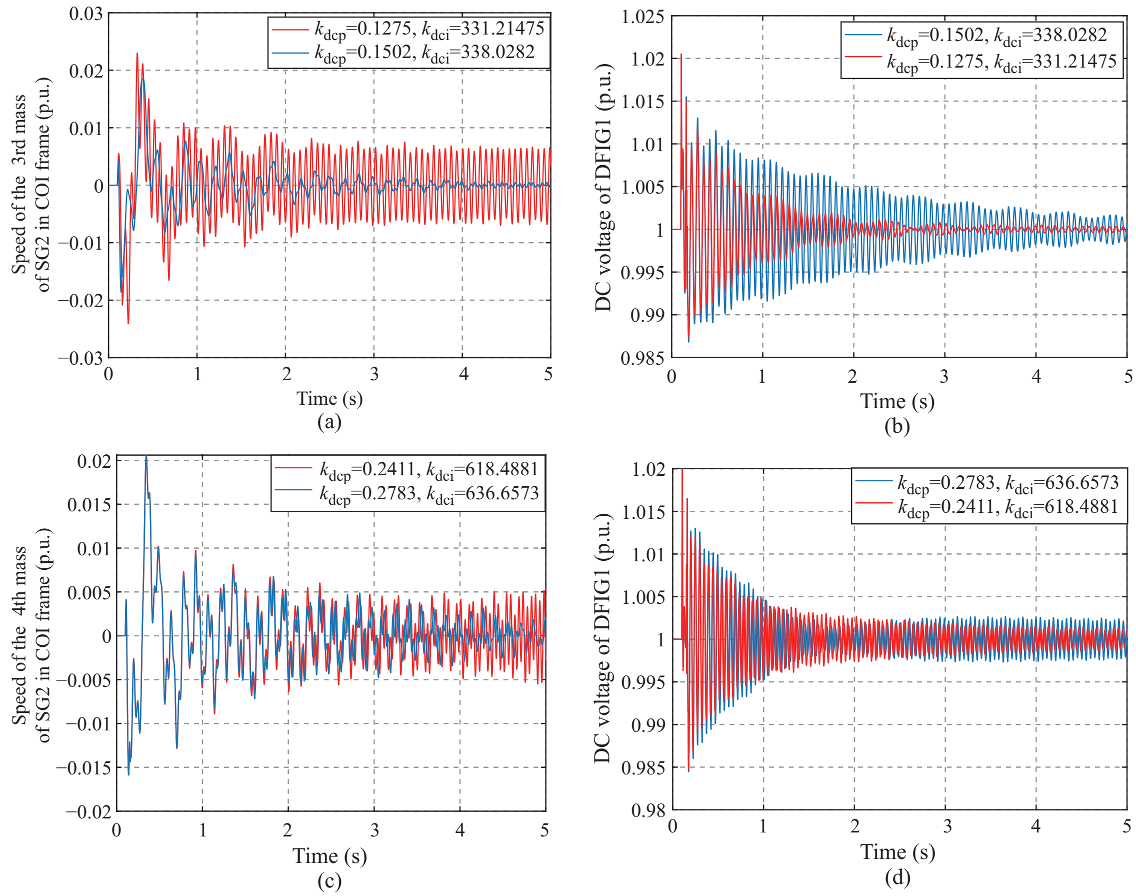

Fig. 8. Results of time domain simulation on the 4-machine 11-bus power system. (a) The difference between the speed of the 3rd mass of SG2 when control parameter $k_{\rm dcp} = 0.1275$, $k_{\rm dci} = 331.21475$ and $k_{\rm dcp} = 0.1502$, $k_{\rm dci} = 338.0282$. (b) The difference between DC voltage of DFIG1 when control parameter $k_{\rm dcp} = 0.1502$, $k_{\rm dci} = 338.0282$and $k_{\rm dcp} = 0.1275$, $k_{\rm dci} = 331.21475$. (c) The difference between the speed of the 4rd mass of SG2 when control parameter $k_{\rm dcp} = 0.2411$, $k_{\rm dci} = 618.4881$ and $k_{\rm dcp} = 0.2783$, $k_{\rm dci} = 636.6573$. (d) The difference between DC voltage of DFIG1 when control parameter $k_{\rm dcp} = 0.2411$, $k_{\rm dci} = 618.4881$ and $k_{\rm dcp} = 0.2783$, $k_{\rm dci} = 636.6573$.

constant and frequency of oscillation of ω_4 and $U_{\rm dc}$ are matched with those indicated by the real and imaginary part of $\hat{\lambda}_{\rm r4-2}$ and $\hat{\lambda}_{\rm dc}$ for $k_{\rm dcp} = 0.2711, k_{\rm dci} = 618.4881$ and $k_{\rm dcp} = 0.2783, k_{\rm dci} = 636.6573$. What's worse, small-signal stability of the entire power system is lost when $k_{\rm dcp} = 0.2711, k_{\rm dci} = 618.4881$.

IV. Conclusion

This paper has studied the mechanism of ASSMA and ASSMR in DFIG-WFs integrated power system and proposed an implicit function based open-loop analysis method for detecting them.

According to analysis in this paper, ASSMA and ASSMR are caused by interaction between open-loop SSO modes of DFIG subsystem and ROPS subsystem as system parameters or operating conditions change. When ASSMA occurs, small-signal stability of the entire power system can be improved On the other hand, if ASSMR is encountered, small-signal stability of the entire power system may be lost [8], which is a novel finding of this paper.

In the proposed open-loop analysis method, partial derivatives of real and imaginary parts of the characteristic equation need to be calculated. But the calculation requires several important parameters of DFIG subsystem, which may be unavailable. As a result, reinforcement learning and least square method are utilized to identify those parameters.

Simulation studies have confirmed the relatively high accuracy of parameter identification. Also, simulation studies have validated estimates of the location of closed-loop SSO modes provided by the proposed method have higher accuracy than those given by the method proposed in [8].

The proposed method can be used for tuning parameters of the controllers of DFIG-WF in order to prevent ASSMR from being excited in the entire power system. Moreover, because the proposed method does not rely on information of the eigenvalues of the state matrix of the entire power system, it may consumes a shorter time for the proposed method to perform small-signal stability analysis when the power system is complex.

Appendix

Linear identification equations:

$$\frac{i_{x\rm s}^i - i_{x\rm s}^{i-1}}{t_i - t_{i-1}} + i_{y\rm s}^i = -120\pi(\omega_{\rm r}^i i_{y\rm r}^i k_1 - V_{x\rm r}^i k_2 + V_{x\rm s}^i k_3 + \omega_{\rm r}^i i_{y\rm s}^i k_4 + i_{x\rm r}^i k_5 - i_{x\rm s}^i k_6)$$

$$\begin{aligned}
\frac{i_{ys}^{i}-i_{ys}^{i-1}}{t_i-t_{i-1}}+i_{xs}^{i} &= 120\pi(\omega_{\mathrm{r}}^{i} i_{xr}^{i} k_1+V_{yr}^{i} k_2-V_{ys}^{i} k_3 \\
&\quad +\omega_{\mathrm{r}}^{i} i_{xs}^{i} k_4-i_{yr}^{i} k_5+i_{ys}^{i} k_6) \\
\frac{i_{xr}^{i}-i_{xr}^{i-1}}{t_i-t_{i-1}}-i_{yr}^{i} &= 120\pi(\omega_{\mathrm{r}}^{i} i_{ys}^{i} k_8+V_{xs}^{i} k_2-V_{xr}^{i} k_9 \\
&\quad +\omega_{\mathrm{r}}^{i} i_{yr}^{i} k_7-i_{xs}^{i} k_{10}+i_{xr}^{i} k_{11}) \\
\frac{i_{yr}^{i}-i_{yr}^{i-1}}{t_i-t_{i-1}}-i_{xr}^{i} &= -120\pi(\omega_{\mathrm{r}}^{i} i_{xs}^{i} k_8-V_{ys}^{i} k_2+V_{yr}^{i} k_9 \\
&\quad +\omega_{\mathrm{r}}^{i} i_{xr}^{i} k_7+i_{ys}^{i} k_{10}-i_{yr}^{i} k_{11}) \\
\frac{i_{xc}^{i}-i_{xc}^{i-1}}{t_i-t_{i-1}}-i_{yc} &= 120\pi((V_{xs}^{i}-V_{xc}^{i})k_{12}-i_{xc}^{i} k_{13}) \\
\frac{i_{yc}^{i}-i_{yc}^{i-1}}{t_i-t_{i-1}}+i_{xc} &= 120\pi((V_{ys}^{i}-V_{yc}^{i})k_{12}-i_{yc}^{i} k_{13}) \\
\frac{\omega_{\mathrm{t}}^{i}-\omega_{\mathrm{t}}^{i-1}}{t_i-t_{i-1}} &= -\omega_{\mathrm{t}}^{i} k_{14}+\omega_{\mathrm{r}}^{i} k_{15}+\left(\frac{P_{\mathrm{m}}}{\omega_{\mathrm{r}}^{i}}-\tilde{T}_{\mathrm{g}}^{i}\right)k_{16} \\
\frac{\omega_{\mathrm{r}}^{i}-\omega_{\mathrm{r}}^{i-1}}{t_i-t_{i-1}} &= \omega_{\mathrm{t}}^{i} k_{17}-\omega_{\mathrm{r}}^{i} k_{18}+\tilde{T}_{\mathrm{g}}^{i} k_{19} \\
&\quad +(i_{xr}^{i} i_{ys}^{i}-i_{yr}^{i} i_{xs}^{i})k_{20} \\
\frac{U_{\mathrm{dc}}^{i}-U_{\mathrm{dc}}^{i-1}}{t_i-t_{i-1}} &= \frac{1}{U_{\mathrm{dc}}^{i}}(V_{xc}^{i} i_{xc}^{i}+V_{yc}^{i} i_{yc}^{i}-V_{xr}^{i} i_{xr}^{i} \\
&\quad -V_{yr}^{i} i_{yr}^{i})k_{21}
\end{aligned} \tag{A1}$$

In (A1), $k_1, k_2, \cdots, k_{21}$ are expressed as:

$$\begin{aligned}
&k_1=\frac{\tilde{L}_{\mathrm{r}}\tilde{L}_{\mathrm{m}}}{\tilde{L}_{\mathrm{m}}^2-\tilde{L}_{\mathrm{r}}\tilde{L}_{\mathrm{s}}},\ k_2=\frac{\tilde{L}_{\mathrm{m}}}{\tilde{L}_{\mathrm{m}}^2-\tilde{L}_{\mathrm{r}}\tilde{L}_{\mathrm{s}}},\ k_3=\frac{\tilde{L}_{\mathrm{r}}}{\tilde{L}_{\mathrm{m}}^2-\tilde{L}_{\mathrm{r}}\tilde{L}_{\mathrm{s}}} \\
&k_4=\frac{\tilde{L}_{\mathrm{m}}^2}{\tilde{L}_{\mathrm{m}}^2-\tilde{L}_{\mathrm{r}}\tilde{L}_{\mathrm{s}}},\ k_5=\frac{\tilde{L}_{\mathrm{m}}\tilde{R}_{\mathrm{r}}}{\tilde{L}_{\mathrm{m}}^2-\tilde{L}_{\mathrm{r}}\tilde{L}_{\mathrm{s}}},\ k_6=\frac{\tilde{L}_{\mathrm{r}}\tilde{R}_{\mathrm{s}}}{\tilde{L}_{\mathrm{m}}^2-\tilde{L}_{\mathrm{r}}\tilde{L}_{\mathrm{s}}} \\
&k_7=\frac{\tilde{L}_{\mathrm{r}}\tilde{L}_{\mathrm{s}}}{\tilde{L}_{\mathrm{m}}^2-\tilde{L}_{\mathrm{r}}\tilde{L}_{\mathrm{s}}},\ k_8=\frac{\tilde{L}_{\mathrm{m}}\tilde{L}_{\mathrm{s}}}{\tilde{L}_{\mathrm{m}}^2-\tilde{L}_{\mathrm{r}}\tilde{L}_{\mathrm{s}}},\ k_9=\frac{\tilde{L}_{\mathrm{s}}}{\tilde{L}_{\mathrm{m}}^2-\tilde{L}_{\mathrm{r}}\tilde{L}_{\mathrm{s}}} \\
&k_{10}=\frac{\tilde{L}_{\mathrm{m}}\tilde{R}_{\mathrm{s}}}{\tilde{L}_{\mathrm{m}}^2-\tilde{L}_{\mathrm{r}}\tilde{L}_{\mathrm{s}}},\ k_{11}=\frac{\tilde{L}_{\mathrm{s}}\tilde{R}_{\mathrm{r}}}{\tilde{L}_{\mathrm{m}}^2-\tilde{L}_{\mathrm{r}}\tilde{L}_{\mathrm{s}}},\ k_{12}=\frac{1}{\tilde{L}_{\mathrm{c}}} \\
&k_{13}=\frac{\tilde{R}_{\mathrm{c}}}{\tilde{L}_{\mathrm{c}}},\ k_{14}=\frac{\tilde{D}_{\mathrm{t}}+\tilde{D}_{\mathrm{tg}}}{2\tilde{H}_{\mathrm{t}}},\ k_{15}=\frac{\tilde{D}_{\mathrm{tg}}}{2\tilde{H}_{\mathrm{t}}} \\
&k_{16}=\frac{1}{2\tilde{H}_{\mathrm{t}}},\ k_{17}=\frac{\tilde{D}_{\mathrm{tg}}}{2\tilde{H}_{\mathrm{g}}},\ k_{18}=\frac{\tilde{D}_{\mathrm{g}}+\tilde{D}_{\mathrm{tg}}}{2\tilde{H}_{\mathrm{g}}} \\
&k_{19}=\frac{1}{2\tilde{H}_{\mathrm{g}}},\ k_{20}=\frac{\tilde{L}_{\mathrm{m}}}{2\tilde{H}_{\mathrm{g}}},\ k_{21}=\frac{1}{\tilde{C}}
\end{aligned} \tag{A2}$$

REFERENCES

[1] W. J. Du, Y. Wang, H. F. Wang, and Q. Fu, "Concept of modal repulsion for examining the sub-synchronous oscillations in power systems," *IEEE Transactions on Power Systems*, vol. 33, no. 4, pp. 4614–4624, Jul. 2018.

[2] W. Heylen, S. Lammens, and P. Sas, *Modal Analysis Theory and Testing*. Belgium: Katholieke Universiteit Leuven Leuven, 1997.

[3] K. R. Padiyar and R. K. Varma, "Damping torque analysis of static VAR system controllers," *IEEE Transactions on Power Systems*, vol. 6, no. 2, pp. 458–465, May 1991.

[4] Y. H. Li, H. Liu, M. X. Yin, and W. Song, "SSR analysis of DFIG-based series-compensated system based on complex torque analysis method," in *2018 International Conference on Power System Technology (POWERCON)*, 2018, pp. 1903–1908.

[5] X. Zhao, S. Gao, and R. Y. Yu, "Damping subsynchronous resonance with SVC based on DTA," in *International Conference on Sustainable Power Generation and Supply (SUPERGEN 2012)*, 2012, pp. 1–5.

[6] Y. P. Song, F. Blaabjerg, and X. F. Wang, "Analysis and active damping of multiple high frequency resonances in DFIG system," *IEEE Transactions on Energy Conversion*, vol. 32, no. 1, pp. 369–381, Mar. 2017.

[7] Y. P. Song, E. Ebrahimzadeh, and F. Blaabjerg, "Analysis of high-frequency resonance in DFIG-based offshore wind farm via long transmission cable," *IEEE Transactions on Energy Conversion*, vol. 33, no. 3, pp. 1036–1046, Sep. 2018.

[8] L. N. Qiu, T. H. Wen, Y. Liu, and Q. H. Wu. "A residue based open-loop modal analysis method for detecting LFMR of PMSG-WFs penetrated power systems," CSEE Journal of Power and Energy Systems, doi: 10. 17775/CSEEJPES.2021.03870.

[9] H. A. Mohammadpour and E. Santi, "SSR damping controller design and optimal placement in rotor-side and grid-side converters of series-compensated DFIG-based wind farm," *IEEE Transactions on Sustainable Energy*, vol. 6, no. 2, pp. 388–399, Apr. 2015.

[10] W. J. Du, Q. Fu, and H. F. Wang, "Strong dynamic interactions between multi-terminal DC network and AC power systems caused by open-loop modal coupling," *IET Generation, Transmission & Distribution*, vol. 11, no. 9, pp. 2362–2374, Jun. 2017.

[11] I. Dobson, "Strong resonance effects in normal form analysis and subsynchronous resonance," in *Bulk Power System Dynamics and Control V*, pp. 563–574, 2001.

[12] I. Dobson, J. Zhang, S. Greene, H. Engdahl, and P. W. Sauer, "Is strong modal resonance a precursor to power system oscillations?" *IEEE Transactions on Circuits and Systems I: Fundamental Theory and Applications*, vol. 48, no. 3, pp. 340– 349, Mar. 2001.

[13] X. L. Liu, Y. Jin, S. Zeng, X. Chen, Y. Feng, S. Q. Liu, and H. L. Liu, "Online identification of power battery parameters for electric vehicles using a decoupling multiple forgetting factors recursive least squares method," *CSEE Journal of Power and Energy Systems*, vol. 6, no. 3, pp. 735–742, Sep. 2020.

[14] K. Y. Wang, J. Chiasson, M. Bodson, and L. M. Tolbert, "A nonlinear least-squares approach for identification of the induction motor parameters," *IEEE Transactions on Automatic Control*, vol. 50, no. 10, pp. 1622–1628, Oct. 2005.

[15] C. X. Jiang, Z. X. Jing, X. R. Cui, T. Y. Ji, and Q. H. Wu, "Multiple agents and reinforcement learning for modelling charging loads of electric taxis," *Applied Energy*, vol. 222, pp. 158–168, Jul. 2018.

[16] F. L. Pagola, I. J. Perez-Arriaga, and G. C. Verghese, "On sensitivities, residues and participations: applications to oscillatory stability analysis and control," *IEEE Transactions on Power Systems*, vol. 4, no. 1, pp. 278–285, Feb. 1989.

[17] T. Kim and H. J. Kim, "Path tracking control and identification of tire parameters using on-line model-based reinforcement learning," in *2016 16th International Conference on Control, Automation and Systems (ICCAS)*, 2016, pp. 215–219.

[18] M. D. Li and Y. J. Ma, "Parameter identification of DC motor based on compound least square method," in *2020 IEEE 5th Information Technology and Mechatronics Engineering Conference (ITOEC)*, 2020, pp. 1107–1111.

[19] M. S. Li, H. M. Zhang, T. Y. Ji, and Q. H. Wu, "Fault identification in power network based on deep reinforcement learning," *CSEE Journal of Power and Energy Systems*, vol. 8, no. 3, pp. 721–731, May 2021.

[20] M. Zhang, C. H. Zhang, H. S. Zhang, C. Peng, and Y. C. Du, "Robust least square method and its application to parameter estimation," in *2007 IEEE International Conference on Automation and Logistics*, 2007, pp. 1483–1486.

[21] P. Kundur, *Power System Stability and Control*. New York: McGraw-Hill Education, 1994.

[22] P. Zhou, D. Lin, C. Lu, M. Rosu, and D. M. Ionel, "An adaptive fixed-point iteration algorithm for finite-element analysis with magnetic hysteresis materials," *IEEE Transactions on Magnetics*, vol. 53, no. 10, pp. 7300705, Oct. 2017.

[23] X. Jiang, W. J. Zeng, and E. Cheng, "A fast fixed point iteration algorithm for sparse channel estimation," in *2011 Third International Conference on Communications and Mobile Computing*, 2011, pp. 405–408.

[24] M. Do Rosário de Pinho and J. F. Rosenblueth, "Mixed constraints in optimal control: an implicit function theorem approach," *IMA Journal of Mathematical Control and Information*, vol. 24, no. 2, pp. 197–218, Jun. 2007.

[25] S. Ichiraku, "A note on global implicit function theorems," *IEEE Transactions on Circuits and Systems*, vol. 32, no. 5, pp. 503– 505, May 1985.

[26] M. Shub, "The implicit function theorem revisited," *IBM Journal of Research and Development*, vol. 38, no. 3, pp. 259–264, May 1994.

[27] S. W. Tento, "The implicit function theorem and robust root locus," in *1991 American Control Conference*, 1991, pp. 869–870.

[28] L. L. Fan, R. Kavasseri, Z. L. Miao, and C. X. Zhu, "Modeling of DFIG-based wind farms for SSR analysis," *IEEE Transactions on Power Delivery*, vol. 25, no. 4, pp. 2073–2082, Oct. 2010.

[29] "First benchmark model for computer simulation of subsynchronous resonance," *IEEE Transactions on Power Apparatus and Systems*, vol. 96, no. 5, pp. 1565–1572, Sep. 1977.

Luonan Qiu received a B.E. degree in Energy Power and Mechanical Engineering from North China Electric Power University, Beijing, China, in 2017. She is currently a Lecturer in the School of Guangdong Pharmaceutical University. Her main research interests include power system stability analysis and control

Tianhao Wen received a B.E. degree in Electrical Engineering from Huazhong University of Science and Technology (HUST), Wuhan, China in 2018. He is currently pursuing the Ph.D degree in South China University of Technology. His research interests include nonlinear observers and power system transient stability analysis.

Yang Liu received a B.E. degree and a Ph.D degree in Electrical Engineering from South China University of Technology (SCUT), Guangzhou, China, in 2012 and 2017, respectively. He is currently a Lecturer in the School of Electric Power Engineering, SCUT. His research interests include the areas of power system stability analysis and control, control of wind power generation systems, and nonlinear control theory. He has authored or co-authored more than 30 peer-reviewed SCI journal papers.

Q. H. Wu received an M.Sc. degree in Electrical Engineering from Huazhong University of Science and Technology, Wuhan, China, in 1981, and a Ph.D. degree in Electrical Engineering from the Queen's University of Belfast (QUB), Belfast, U.K., in 1987. He worked as the Chair Professor at Liverpool University from 1995 to 2012. He is currently a Distinguished Professor and the Director of Energy Research Institute, South China University of Technology, Guangzhou, China. He is a Life Fellow of IEEE, Fellow of IET, CSEE Fellow, Fellow of AAIA, and Chartered Engineer. He has authored and coauthored more than 350 journal papers, 20 book chapters and 4 research monographs published by Springer Nature. His research interests include nonlinear adaptive control, mathematical morphology, artificial intelligence, and power system control and operation.